



**UNIVERSIDAD DE INVESTIGACIÓN DE TECNOLOGÍA  
EXPERIMENTAL YACHAY**

**Escuela de Ciencias Químicas e Ingeniería**

**TÍTULO: Moringa Oleifera Fiber and Ecuadorian Montmorillonite  
Composite for Removal Potentially Toxic Metals**

Trabajo de integración curricular presentado como requisito para la obtención del  
título de Químico

**Autor:**

Soto Villegas Cynthia Elizabeth

**Tutor:**

PhD. López González Flor Alba

Urcuquí – Julio, 2020

**SECRETARÍA GENERAL**  
**(Vicerrectorado Académico/Cancillería)**  
**ESCUELA DE CIENCIAS QUÍMICAS E INGENIERÍA**  
**CARRERA DE QUÍMICA**  
**ACTA DE DEFENSA No. UITEY-CHE-2020-00042-AD**

A los 17 días del mes de julio de 2020, a las 11:00 horas, de manera virtual mediante videoconferencia, y ante el Tribunal Calificador, integrado por los docentes:

<b>Presidente Tribunal de Defensa</b>	Dr. BASTARDO GONZÁLEZ, ERNESTO LUIS , Ph.D.
<b>Miembro No Tutor</b>	Mgs. DE LIMA ELJURI, LOLA MARIA
<b>Tutor</b>	Dra. LOPEZ GONZALEZ, FLORALBA AGGENY , Ph.D.

El(la) señor(ita) estudiante **SOTO VILLEGAS, CYNTHIA ELIZABETH**, con cédula de identidad No. **0106646243**, de la **ESCUELA DE CIENCIAS QUÍMICAS E INGENIERÍA**, de la Carrera de **QUÍMICA**, aprobada por el Consejo de Educación Superior (CES), mediante Resolución **RPC-SO-39-No.456-2014**, realiza a través de videoconferencia, la sustentación de su trabajo de titulación denominado: **Moringa Oleifera Fiber and Ecuadorian Montmorillonite Composite for Removal Potentially Toxic Metals**, previa a la obtención del título de **QUÍMICO/A**.

El citado trabajo de titulación, fue debidamente aprobado por el(los) docente(s):

<b>Tutor</b>	Dra. LOPEZ GONZALEZ, FLORALBA AGGENY , Ph.D.
--------------	--

Y recibió las observaciones de los otros miembros del Tribunal Calificador, las mismas que han sido incorporadas por el(la) estudiante.

Previamente cumplidos los requisitos legales y reglamentarios, el trabajo de titulación fue sustentado por el(la) estudiante y examinado por los miembros del Tribunal Calificador. Escuchada la sustentación del trabajo de titulación a través de videoconferencia, que integró la exposición de el(la) estudiante sobre el contenido de la misma y las preguntas formuladas por los miembros del Tribunal, se califica la sustentación del trabajo de titulación con las siguientes calificaciones:

Tipo	Docente	Calificación
Miembro Tribunal De Defensa	Mgs. DE LIMA ELJURI, LOLA MARIA	10,0
Presidente Tribunal De Defensa	Dr. BASTARDO GONZÁLEZ, ERNESTO LUIS , Ph.D.	10,0
Tutor	Dra. LOPEZ GONZALEZ, FLORALBA AGGENY , Ph.D.	10,0

Lo que da un promedio de: **10 (Diez punto Cero)**, sobre 10 (diez), equivalente a: **APROBADO**

Para constancia de lo actuado, firman los miembros del Tribunal Calificador, el/la estudiante y el/la secretario ad-hoc.

*Certifico que en cumplimiento del Decreto Ejecutivo 1017 de 16 de marzo de 2020, la defensa de trabajo de titulación (o examen de grado modalidad teórico práctica) se realizó vía virtual, por lo que las firmas de los miembros del Tribunal de Defensa de Grado, constan en forma digital.*

**SOTO VILLEGAS, CYNTHIA ELIZABETH**  
**Estudiante**

**Dr. BASTARDO GONZÁLEZ, ERNESTO LUIS , Ph.D.**  
**Presidente Tribunal de Defensa**

**ERNESTO LUIS  
 BASTARDO  
 GONZALEZ**

Firmado digitalmente por  
 ERNESTO LUIS BASTARDO  
 GONZALEZ  
 Fecha: 2020.07.17 13:15:05  
 -05'00'

FLORALBA AGGENY LOPEZ  
GONZALEZ

Firmado digitalmente por FLORALBA AGGENY LOPEZ GONZALEZ  
Nombre de reconocimiento (DN): c=EC, o=BANCO CENTRAL DEL ECUADOR,  
ou=ENTIDAD DE CERTIFICACION DE INFORMACION-ECIBCE, l=-QUITO,  
serialNumber=0000269534, cn=FLORALBA AGGENY LOPEZ GONZALEZ  
Fecha: 2020.07.19 14:08:56 -05'00'

Dra. LOPEZ GONZALEZ, FLORALBA AGGENY , Ph.D.  
**Tutor**

Mgs. DE LIMA ELJURI, LOLA MARIA  
**Miembro No Tutor**

LOLA MARIA DE LIMA ELJURI  
Digitally signed by  
LOLA MARIA DE LIMA  
ELJURI  
Date: 2020.07.17  
14:29:03 -05'00'

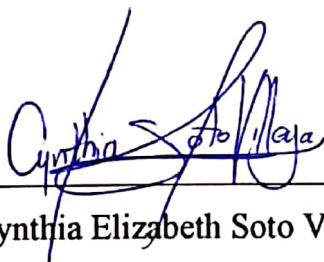
ESCOBAR LANDAZURI, ANA MARIA  
**Secretario Ad-hoc**

 Firmado electrónicamente por:  
**ANA MARIA  
ESCOBAR  
LANDAZURI**

# Autoría

Yo, **CYNTHIA ELIZABETH SOTO VILLEGAS**, con cédula de identidad 0106646243, declaro que las ideas, juicios, discusiones, valoraciones, interpretaciones, consultas bibliográficas, definiciones y conceptualizaciones expuestas en el presente trabajo; así cómo, los procedimientos y herramientas utilizadas en la investigación, son de absoluta responsabilidad de el/la autora (a) del trabajo de integración curricular. Así mismo, me acojo a los reglamentos internos de la Universidad de Investigación de Tecnología Experimental Yachay.

Urcuquí, Julio del 2020.



---

Cynthia Elizabeth Soto Villegas

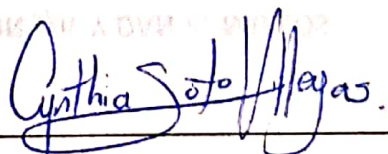
CI: 0106646243

# Autorización de publicación

Yo, **CYNTHIA ELIZABETH SOTO VILLEGAS**, con cédula de identidad 0106646243, cedo a la Universidad de Tecnología Experimental Yachay, los derechos de publicación de la presente obra, sin que deba haber un reconocimiento económico por este concepto. Declaro además que el texto del presente trabajo de titulación no podrá ser cedido a ninguna empresa editorial para su publicación u otros fines, sin contar previamente con la autorización escrita de la Universidad.

Asimismo, autorizo a la Universidad que realice la digitalización y publicación de este trabajo de integración curricular en el repositorio virtual, de conformidad a lo dispuesto en el Art. 144 de la Ley Orgánica de Educación Superior.

Urcuquí, Julio del 2020.



---

Cynthia Elizabeth Soto Villegas

CI: 010664624

*This work is dedicated to my parents, Ramiro and Elizabeth, for supporting me since I was born, for being a role model they are in my life and for all their unconditional love.*

*To my brothers, Fabián, Danilo, José and Javier, for trusting in my talent and capacity, because it does not matter how much time passes, I can always count on them.*

*To my nephew, Joaquín, so that he never gives up on his goals and learns that all his dreams can be achieved with dedication and passion in what we do.*

*To my friends, for all these years of friendship with which we grew and learned together. Especially to André, for his honest friendship, support, love and adventures.*

*Cynthia Elizabeth Soto Villegas.*

# Acknowledgment

*First and foremost, I am very grateful with God for His unconditional love, blessings and opportunities He has given me, for the strength to overcome every difficulty and, especially, for introducing wonderful people in my way, who have contributed in my life to reach my dreams.*

*Of course, I would like to express my sincere gratitude to my admirable research supervisor, Floralba López, who always believed in me and with her assistance and support in each step of this work, made possible this thesis. I want to thank you for all the understanding and guidance during this time.*

*Also, I would like to thank Ph.D. Efraín Rubio and Ph.D. José Ángel Rivera to allow our research work in Benemérita Universidad Autónoma de Puebla's labs, because your collaboration was of vital importance for this work.*

*An especial thanks to my friends Clara, Lisandra y Bernardo for being by my side all these years, giving me their support, love, and understanding to overcome the hard situations during this work and all these academic years.*

*Finally, to the two people to whom I owe everything, my parents, Elizabeth Villegas and Ramiro Soto, who have taught me to be strong, persistent, brave and always being by my side. To my brothers, Fabián, Danilo, and José who have always believed in me, even when I did not, thanks for being my role model and show me that I always can achieve what I propose. Thanks to my family for all your love.*

*Cynthia Elizabeth Soto Villegas*

# Resumen

El cromo hexavalente, Cr(VI), es un metal potencialmente tóxico encontrado en aguas residuales de actividades industriales. Amenaza la salud humana y el medio ambiente, por lo tanto, su remoción es necesaria en la industria. Este trabajo está enfocado en la síntesis de tres compósitos para evaluar su capacidad de adsorción, los compósitos fueron preparados a partir de la arcilla montmorillonita natural, con la fibra de semillas de *Moringa oleífera* (MOSP) en proporciones  $g_{\text{MOSP}}/g_{\text{arcilla}}$  de 1.0, 0.6 y 0.2. Los materiales de partida y los compósitos fueron caracterizados a través de Espectroscopía Infrarroja (FT-IR), Espectroscopía de fotoemisión electrónica por rayos X (XPS), Difracción de rayos X (XRD), Microscopía Electrónica de Barrido (SEM), Espectroscopía de rayos X de Dispersión de Energía (EDX), y Análisis Superficial. Se evaluó la capacidad de adsorción de los materiales usando Espectroscopía Ultravioleta-visible (UV-Vis), y mediante la variación diferentes parámetros, tales como el pH de la solución, la concentración inicial de Cr(VI) y el tiempo de contacto adsorbente-solución.

Se encontró que la fibra MOSP y el compósito conteniendo la mayor proporción de MOSP (Comp-11), presentaron los mayores porcentajes de remoción de Cr(VI), alcanzando valores de 56% y 25% de remoción, respectivamente. El comportamiento de los sistemas de adsorción fue ajustado con los modelos de Langmuir y Freundlich, así como también una propuesta del modelo de BET para sistemas líquidos, sugiriendo que el proceso de adsorción se debe a la combinación de procesos de quimisorción y fisorción. Particularmente para el caso de los compósitos, el ajuste a los modelos mencionados indica la formación de una monocapa sobre la superficie del adsorbente, que podría ser atribuido a la presencia de MOSP en la superficie, resultando ser el principal responsable de las reacciones químicas entre el adsorbato y la superficie del adsorbente. El bajo costo y el bajo impacto negativo sobre el medioambiente, además de su capacidad de adsorción, son propiedades de atribuibles a la montmorillonita y las semillas de *Moringa oleífera*, y por lo tanto los compósitos obtenidos a partir de ellos resultan una interesante alternativa opción en el campo de los adsorbentes naturales.

Palabras clave: montmorillonite, *Moringa oleífera*, adsorción, remoción de Cr(VI), adsorbentes naturales.

# Abstract

Hexavalent chromium, Cr(VI), is a potentially toxic metal found in wastewater from industrial activities. It threatens human health and the environment, therefore, its removal is necessary in the industry. This work is focused on synthesizing three composites to evaluate their adsorption capacity, the composites were prepared from natural montmorillonite clay with *Moringa oleifera* seed powder (MOSP) fiber in  $g_{\text{MOSP}}/g_{\text{clay}}$  ratios of 1.0, 0.6 and 0.2. The raw materials and the composites were characterized by Infrared Spectroscopy (FT-IR), X-ray electron Photoemission Spectroscopy (XPS), X-ray Diffraction (XRD), Scanning Electron Microscopy (SEM), Energy-Dispersive X-ray Spectroscopy (EDX), and Surface Analysis. By adsorption analysis using Ultraviolet-Visible Spectroscopy (UV-Vis), the adsorption capacity of the materials was evaluated, by varying parameters, such as the pH of the solution, the initial concentration of Cr(VI) and adsorbent-solution contact time.

It was found that the MOSP fiber and the composite containing the highest proportion of MOSP (Comp-11), had the highest Cr(VI) removal yield, reaching 56% and 25% removal values, respectively. The behavior of the adsorption systems was fitted with Langmuir and Freundlich models, as well as by a proposal of the BET model for liquid systems, suggesting that the adsorption process is due to the combination of chemisorption and physisorption processes. Particularly in the case of prepared composites, the fit to the mentioned models indicates the formation of a monolayer on the surface of the adsorbent, which could be attributed to the presence of MOSP on the surface, this being the main responsible for the chemical reactions between the adsorbate and the adsorbent surface. The low cost and low negative impact on the environment, in addition to their adsorption capacity, are properties attributable to montmorillonite and *Moringa oleifera* seeds, and therefore the compounds obtained from them are an interesting alternative in the field of natural adsorbents of potentially toxic metal species.

Keywords: montmorillonite, *Moringa oleifera*, adsorption, Cr(VI) removal, natural adsorbents.

# Contents

<b>Acknowledgment</b>	<b>vii</b>
<b>Resumen</b>	<b>viii</b>
<b>Abstract</b>	<b>ix</b>
<b>Introduction</b>	<b>16</b>
1.1 Water: a human resource.	16
1.2 Montmorillonite Clay.	18
1.3 <i>Moringa Oleifera</i>	20
<b>Problem statement</b>	<b>22</b>
<b>Objectives</b>	<b>25</b>
3.1 General objective	25
3.2 Specific objectives	25
<b>Theoretical Background</b>	<b>26</b>
4.1 Adsorption	26
4.2 Adsorption Models	26
4.2.1 Langmuir Model	27
4.2.2 Freundlich Model	28
4.2.3 BET Model	28
4.3 <i>Moringa oleifera</i> in metal ions adsorption	30
4.4 Montmorillonite clay in metal adsorption	31
4.5 Clay concentration	31
4.5.1 Carbonates removal	32

<b>Methodology</b>	<b>33</b>
5.1 Materials and Chemical Reagents	33
5.2 Activated Na-montmorillonite clay preparation	33
5.2.1 Concentration of the montmorillonite clay	33
5.2.2 Montmorillonite acid activation	34
5.1.3 Ion exchange on the activated montmorillonite clay	35
5.3 Preparation of <i>Moringa oleifera</i> seed powder solution	35
5.3.1 Oil extraction from <i>Moringa oleifera</i> seeds	35
5.3.2 Extraction of de-oiled MOSP solution	36
5.4 Composite preparation	36
5.5 Characterization of the samples	37
5.5.1 Fourier - Transform Infrared (FTIR) Spectroscopy Analysis	37
5.5.2 Scanning Electron Microscopy (SEM) and Energy Dispersive X-Ray Spectroscopy (EDX) Analysis	37
5.5.3 X-ray Diffraction (XRD) Analysis	37
5.5.4 X-ray Photoemission Spectroscopy (XPS) Analysis	37
5.5.5 Surface Analysis	38
5.6 Adsorption Capacity Evaluation	38
5.6.1 Calibration Curve Construction	39
5.6.2 Determination of suitable parameters	39
5.6.3 Variation of initial concentration Cr(VI) - Adsorption Isotherms	40
<b>Results and Discussion</b>	<b>42</b>
6.1 FT-IR Analysis	42
6.2 SEM and EDS Analysis	46

6.3 XRD Analysis _____	47
6.4 XPS Analysis _____	50
6.5 Surface Area Analysis _____	55
6.6 Adsorption Analysis _____	55
6.6.1 Effect of the pH _____	56
6.6.2 Effect of contact time _____	58
6.6.3 Effect of initial metal ion concentration _____	59
6.6.4 Adsorption isotherms _____	60
<b>Conclusions</b> _____	<b>67</b>
<b>References</b> _____	<b>69</b>
<b>Annex 1</b> _____	<b>77</b>
FT-IR Analysis for Composites _____	77
<b>Annex 2</b> _____	<b>78</b>
Adsorption Isotherms by Modified BET model for composites Comp-16 and Comp-12.____	78
<b>Annex 3</b> _____	<b>79</b>
Removal of Cr(VI) ions (%) of all the materials analyzed. _____	79

# List of Figures

Figure 1.1 Earth's water distribution. Taken from USGS <sup>4</sup> . _____	16
Figure 1.2 Sketch of a layer structure in a Montmorillonite. Extracted from Peshawar <sup>12</sup> _____	18
Figure 1.3 Description of Moringa oleifera parts. A. Pinnate leaves. B. Fruit. C. Seeds. Extracted from Revista Mexicana de Biodiversidad <sup>17</sup> . _____	20
Figure 4.1 Types of adsorption isotherms for different materials. Extracted from Aligizaki <sup>49</sup> _	29
Figure 6.1 FT-IR spectra of activated Na-montmorillonite _____	42
Figure 6.2 FT-IR spectra for activated Na-montmorillonite and commercial montmorillonite. _____	43
Figure 6.3 FT-IR spectra of MOSP _____	44
Figure 6.4 FT-IR spectra of Composite 1.1 _____	45
Figure 6.5 SEM images A. Composite 1.1 and B. Activated Na-montmorillonite. _____	46
Figure 6.6 XRD diffractogram for activated Na-montmorillonite _____	47
Figure 6.7 XRD diffractogram of A. Database montmorillonite and B. Activated Na-montmorillonite _____	48
Figure 6.8 XRD diffractogram for A. Composite 1.1 and B. Activated Na-montmorillonite. ___	49
Figure 6.9 XPS pattern for activated Na-montmorillonite, Composite with MOSP and Composite with Cr(VI) adsorption. _____	50
Figure 6.10 XPS pattern for Oxygen (O1s) _____	51
Figure 6.11 XPS pattern for Carbon (C1s) _____	52
Figure 6.12 XPS pattern for Nitrogen (N1s) _____	53
Figure 6.13 XPS pattern for Chromium (Cr2p3/2) _____	54
Figure 6.14 Calibration curve for Cr(VI) _____	56
Figure 6.15 Oxides reaction at acidic pH. Extracted from Akar et. al <sup>74</sup> . _____	57

Figure 6.16 Effect of pH on the adsorption of Cr(VI) ions. Contact time: A. 1 hour B. 17 hours.	57
<hr/>	
Figure 6.17 Effect of contact time in a 100ppm solution at 1h, 3h, and 17h.	59
Figure 6.18 Effect of the initial Cr (VI) concentration in the adsorption capacity (mg/g) and removal efficiency (R %) of Cr (VI) ions (adsorbent dosage: 10 g/L, pH: 2 and reaction time: 3 h)	60
<hr/>	
Figure 6.19 Isotherm data fit adjusted to isotherms Langmuir and Freundlich for A. activated Na-montmorillonite and B. MOSP	62
<hr/>	
Figure 6.20 Isotherm data fit adjusted to isotherms Langmuir and Freundlich for A. activated Na-montmorillonite and B. MOSP at higher concentrations	62
<hr/>	
Figure 6.21 Isotherm data fit adjusted to isotherms Langmuir and Freundlich for A. Composite 1.1, B. Composite 1.6 and C. Composite 1.2	63
<hr/>	
Figure 6.22 Isotherm data fit adjusted to isotherms Langmuir and Freundlich for A. Composite 1.1, B. Composite 1.6 and C. Composite 1.2 at higher concentrations.	64
<hr/>	
Figure 6.23 BET Adsorption isotherms: A. Conventional BET B. BET for liquids. For Comp. 1.1.	65
<hr/>	
Figure 7.1 FT-IR spectra of Composite 1.6	77
<hr/>	
Figure 7.2 FT-IR spectra of Composite 1.2	77
<hr/>	
Figure 7.3 BET Adsorption isotherms: A. Conventional BET B. BET for liquids. For Comp. 1.6	78
<hr/>	
Figure 7.4 BET Adsorption isotherms: A. Conventional BET B. BET for liquids. For Comp. 1.2	78
<hr/>	

# List of Tables

Table 2.1 Permissible Limit for metal concentrations in freshwater and water for human consumption and domestic use. Extracted from Norma de Calidad Ambiental y de Descarga de Efluentes: Recurso Agua <sup>46</sup> .	24
Table 4.1 Types of adsorption isotherms for different materials <sup>49,50</sup> .	29
Table 6.1 Chemical composition of the surfaces of Activated Na-montmorillonite (AMN), MOSP, Comp-11, Comp-16 and Comp-12 analyzed by EDX.	47
Table 6.2 BET surface areas from Nitrogen adsorption on AMN and functionalized composite.	55
Table 6.3 Adsorptive capacity obtained for each adsorbent evaluated for all of the chromium solutions.	61
Table 6.4 Values for fit parameters associated with Langmuir Adsorption Isotherm for the different analyzed adsorbents.	64
Table 6.5 Values for fit parameters associated with both modified BET-models: Classical BET model using $x = C_e/C_s$ and modified BET-model for liquids, for the different analyzed composites.	66
Table 7.1 Removal of Cr(VI) ions of all materials used (%)	79

# Chapter 1

## Introduction

### 1.1 Water: a human resource.

Water is an essential element for the sustainability and development of life on Earth. An average person requires around 50 liters of water per day, to fulfill their biological needs and domestic activities<sup>1</sup>. To guarantee access to safe drinking water is a political concern at national, regional and local levels. It ensures the health safety of the population, given that, the lack of it promotes the proliferation of diseases<sup>2</sup>. Children and young people are the most vulnerable to get water-related diseases like diarrhea, trachoma, schistosomiasis, etc. preventable diseases<sup>1</sup> which due to the absence of drinking water and suitable sanitation, nowadays are the cause of 2 million to 5 million deaths per year<sup>3</sup>. The Earth is mostly constituted by water, covering almost 70 percent of it. However, 96.5 percent of the hydrosphere is saline water from the oceans and just 2.5 percent is freshwater which, around 68 percent of it is enclosed in ice caps, glaciers, and snow<sup>4,5</sup> (Fig. 1.1).

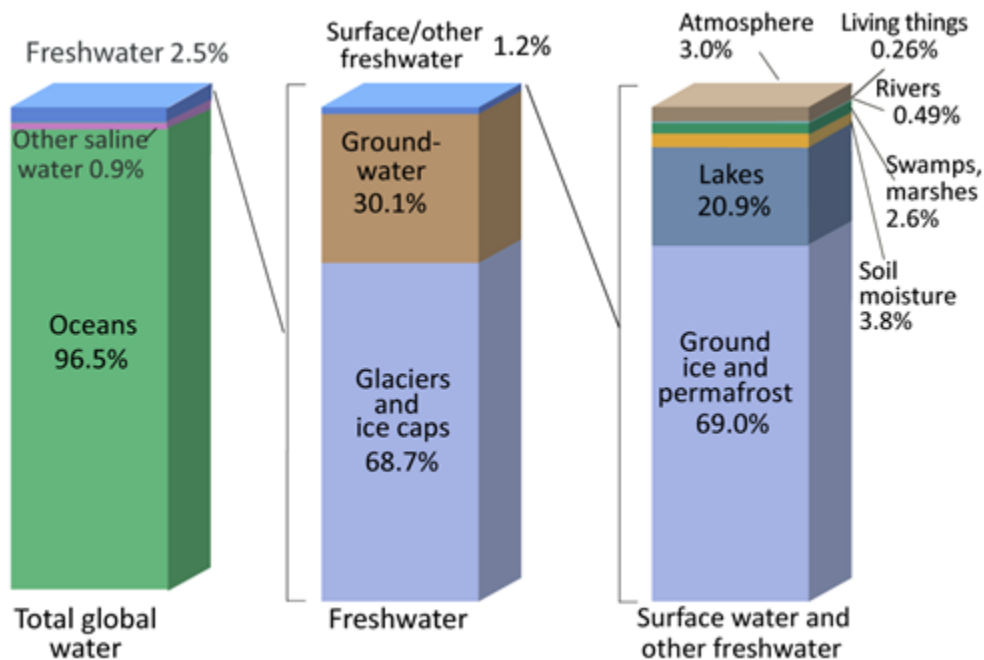


Figure 1.1 Earth's water distribution. Taken from USGS<sup>4</sup>.

Freshwater complies an important role in preserving life, how it is used and dispose of is an environmental issue of international concern<sup>6</sup>. Especially, due to the high level of water's vulnerability to contamination<sup>5</sup>, which can be polluted by different sources as microbial, chemical, physical or biotic factors<sup>2</sup>. The main reason for water pollution is due to anthropogenic activities, and the rapid increase in human population makes the situation even worse<sup>6</sup>. Overcrowded areas, industrial activities, discharge of fields, production and use of plastic, chemicals, debris, etc., are just a few examples of the damage to the planet's sources of water<sup>5</sup>.

Failure to guarantee access to drinking water and sanitation has repercussions in diverse social aspects; for example, economically speaking, the health implications related to the consumption of unsafe water represent a rise in public spending<sup>2</sup>. For this reason, developing strategies for the conservation and management of drinking water is of political concern. At the moment of establishing water management policies it is essential to start by determining if the water will be used for domestic, industry, transport, energy or even agriculture activities<sup>1</sup>.

Nowadays, several water-treatment systems are ensemble worldwide by considering different factors as population, costs of implementation and maintenance, and the community's behavior to ensure the effectiveness of the system over the long-term<sup>7</sup>. Depending on the scope of the system, it can be applied at home or for a whole community. For household water treatment, there are three main methods: boiling the water, slow sand filter, and domestic chlorination. While, for a community, there are other options like: storage and sedimentation, up-flow roughing filter, complete water treatment plants and chlorination in piped water-supply systems<sup>8</sup>. Despite the efforts to provide access to drinking water and sanitation to all nations, new threats are found during the process, such as economic troubles, lack of workforce or human resources, minimum political interest, absence of access roads, etc<sup>3</sup>. Thus, there are numerous communities around the world without access to drinking water waiting for a solution to their hard reality<sup>1</sup>. Scientific research suggests the possibility of using natural technologies, such as: soil filters, treatment wetlands, aerobic and anaerobic treatments, as the first solution to this matter<sup>9</sup>. However, the search for natural, replicable and accessible options is still being pursuit.

This work strives to contribute to this search by developing a composite of montmorillonite clay and *Moringa oleifera* seed to use as a natural adsorbent in the treatment of water. In the next sections we will explore these two components and why they were selected for this purpose.

## 1.2 Montmorillonite Clay.

Clays are primarily composed by oxygen, silica, water, and alumina and/or magnesium (in some cases both), besides, depending on the nature of the clay there could be some amounts of calcium, potassium, and sodium, or even alumina or magnesium could be replaced by iron atoms<sup>10</sup>. Clays are natural materials that have been gaining popularity in diverse fields, due to its low cost, porosity, climatic versatility, plasticity depending on its content of water or rigidity in its dry appearance<sup>11,12</sup>. The clays classification, according to their layered structure, consists of four main groups: kaolinite, mica, chlorite, and smectite<sup>13</sup>. The smectite group are aluminosilicate determined by a layer type 2:1, i.e., one octahedral alumina sheet contained between two tetrahedral silica sheets<sup>11,14</sup> (Figure 1.2).

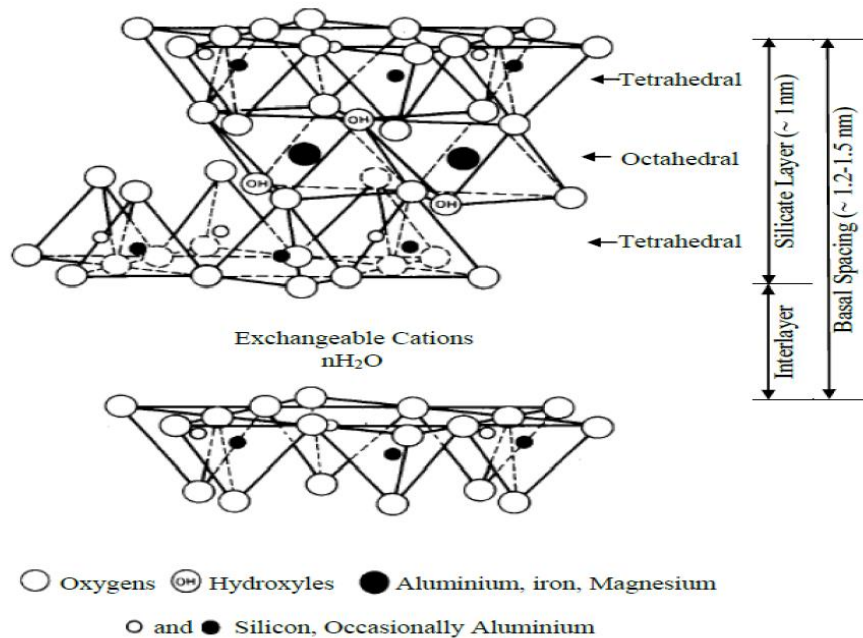


Figure 1.2 Sketch of a layer structure in a Montmorillonite. Extracted from Peshawar<sup>12</sup>

In the smectite group, the montmorillonite type tends to have more octahedral than tetrahedral substitutions<sup>10</sup>. Montmorillonite clay is named after the place where it was

discovered, Montmorillon in the Vienne prefecture of France. However, its principal deposits are found worldwide in the following countries: China, Pakistan, Georgia, Russia, Peru, Ecuador, and USA. In nature, it is mostly found in the bentonite clay, a rock composed primarily by montmorillonite, but that also contains crystalline quartz, cristobalite, and feldspar<sup>11</sup>.

Montmorillonite clay has characteristics that are of interest and application in the material science field such as: its cation exchange skill, its capacity to form thixotropic gels, and its facility to absorb water molecules inside its structure (increasing its volume 12 or 15 times)<sup>14</sup>. Due to isomorphous substitutions<sup>11</sup>, the lattice in montmorillonite clay has a negative charge, which can be countered with the presence of  $\text{Na}^+$ ,  $\text{Ca}^{2+}$ ,  $\text{K}^+$ , or  $\text{Mg}^{2+}$  as interlayer cations. The weak binding of these cations allows them to be exchangeable and grants to the montmorillonite clay its great cation exchange capacity ( $\approx 100 \text{ meq}/100 \text{ g}$ )<sup>14</sup>.

Cation Exchange Capacity (CEC) can be defined as the portion of cations reversibly adsorbed by the interlayer and edges of the clay<sup>12</sup>. It is this capacity which makes montmorillonite clay act as a powerful natural adsorbent with numerous applications<sup>14</sup>. However, the ion exchange interaction predominates when the adsorbed substance does not exceed the clay's CEC value; when it exceeds the clay's CEC value, another interactions like van der Waals weak bonding, hydrophobic effects or H-bonding start to play an important role in the adsorption capacity of the clay<sup>15</sup>. Besides cation exchange capacity, the efficiency of adsorption of the clay is determined by: the size particle of the clay, its crystallinity, and the nature of the adsorbed ion<sup>10</sup>.

Adsorption systems are commonly used for water treatment for its efficiency – cost relation, however, the materials frequently employed are synthetic, non-degradable and its production involves an extra cost<sup>16</sup>. In this work the montmorillonite clay is studied as one of the components in an alternative natural and biodegradable adsorbent for the removal of harmful substances from aqueous solutions<sup>15</sup>. Its low cost, availability, and adaptability make montmorillonite clay a suitable option for the synthesis of composites for water treatment<sup>11</sup>.

In the next section, it will take a look at *Moringa oleifera*, the other component in the adsorbent being developed.

### 1.3 *Moringa Oleifera*

*Moringa*, an Indian native plant<sup>17</sup>, belongs to the *Moringaceae* family in the order *Brassicales*<sup>18</sup>. The *Moringaceae* family has only one genus, the *Moringa*, with thirteen recognized species: *M. oleifera*, *M. arborea*, *M. borziana*, *M. concanensis*, *M. drouhardii*, *M. hildebrandtii*, *M. longituba*, *M. ovalifolia*, *M. peregrina*, *M. pygmaea*, *M. rivae*, *M. ruspoliana*, and *M. stenopetala*<sup>17</sup>. The possibility of using the whole plant for research has made *Moringa oleifera* the specie most studied to date; its leaves and pods have high nutritional levels, while its flowers and roots have medicinal applications, and its seeds are effective in water treatments<sup>19</sup>.

*Moringa oleifera* is a tropical plant, which also grows in semi-arid zones like: Africa, Arabia, South East Asia, the Pacific, and Caribbean Islands and South America<sup>20</sup>. It can reach 12 meters of height and is easily recognizable by its pinnate leaves, which can reach a length of 60 centimeters. Also, its fruits sprout in long pods within which seeds are found, these beige seeds have a diameter of 1.5 – 3 centimeters and are covered by a dark brown shell (Figure 1.3)<sup>17,18</sup>.

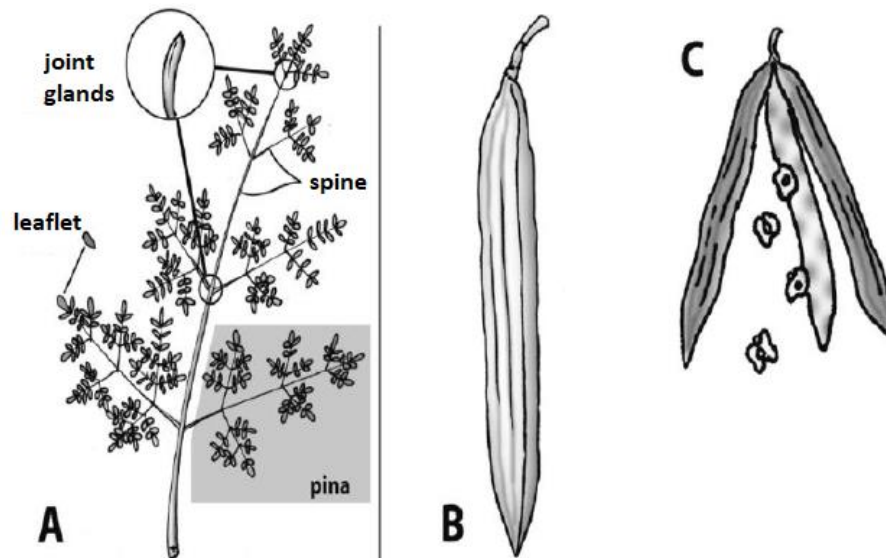


Figure 1.3 Description of *Moringa oleifera* parts. A. Pinnate leaves. B. Fruit. C. Seeds. Extracted from *Revista Mexicana de Biodiversidad*<sup>17</sup>.

Several properties are attributed to *Moringa oleifera* seeds, e.g. the presence of cationic polyelectrolytes gives these seeds the property of flocculant – coagulant which is crucial for the treatment of turbid water<sup>18</sup>. This property is associated with the hydrophilic polar amino acids found in the seeds, some of them have been identified as glutamic acid, arginine, aspartic acid,

lysine, and histidine<sup>21</sup>. When these amino acids come into contact with water, they are ionized and the coagulation takes place because neutralizing their charges destabilizes colloids. Then, the flocculation occurs by the agglomeration of small particles with a neutral charge, to increase their weight and volume, therefore, increasing their density and favoring the precipitation process<sup>22</sup>.

The turbidity and color of sewage water are due to the presence of colloids that possess a negative surface charge, repelling each other and avoiding their flocculation<sup>23</sup>. Hence, the employment of a coagulant in the first step for water treatment is essential for the efficiency of the following steps of the process<sup>24</sup>. At present, coagulants as aluminum sulfate, ferric chloride or even, coagulant polymers are preferred in the water treatment process<sup>25</sup>. Although aluminum sulfate is the most used<sup>22</sup>, some studies have found a relation between neurofibrillary degeneration and aluminum concentrations in mammals organisms<sup>24,26</sup>. These findings relate the aluminum sulfate with the development of Alzheimer's disease<sup>26</sup>. For this reason, research for alternative, natural and biodegradable coagulants have increased. In the search to find a coagulant that does not increase aluminum's concentration in drinking water, alters its pH nor rises the residual organic concentration<sup>24</sup> *Moringa oleifera*'s seed has been proposed.

*Moringa oleifera* also shows an antibiotic capacity as a result of the presence of pterygospermin in its composition, this compound dissociates in benzyl isothiocyanate, a lethal substance against *Micrococcus pyogenes var. aureus*, *Escherichia coli*, *pseudomonas*, etc.<sup>27</sup> Besides, *Moringa oleifera* presents active agents as 4-(4'-O-acetyl- $\alpha$ -L-rhamnopyranosyloxy) benzyl isothiocyanate, 4-( $\alpha$ -L-rhamnopyranosyloxy)benzyl isothiocyanate, niazimicin, and 4-( $\alpha$ -L-rhamnopyranosyloxy) benzyl glucosinolate<sup>28-30</sup>, which provides it the capacity of reducing the concentrations of mesophilic aerobic bacteria, mesophilic fungi and fecal coliform bacteria (pathogens) found in raw water<sup>23</sup>.

## Chapter 2

# Problem statement

Water is a primordial resource for the development of life, however, it is being threatened by human activities like industrial processes, urbanization, agriculture, shipping, mining, etc., the same activities that mark progress for human kind<sup>18,20,31</sup>. Of these activities, the main source of water pollution are the industrial processes, wastewater generated by these processes present an accumulation of dangerous chemical compounds, commonly called heavy metals<sup>32</sup>, which are the most biologically harmful substances found in wastewater<sup>31</sup>. The term “heavy” should be related to the density, or atomic number or atomic weight of involved elements; however, in the literature they are referred to metals that generate some toxic effects on the environment and biological organisms. Therefore, to avoid this misunderstanding, the term “potentially toxic” is more accurate when referring to these metals<sup>18</sup>. These potentially toxic metals, even in small traces, are considered the most harmful water pollutant in a large body of water. For their propensity to accumulate inside the organism of living beings and generating harmful effects in their organs<sup>16</sup>, they represent a threat to the environment and public health.

In Ecuador, several industries require large amounts of water for their operations and among them the most polluting are the chemical industries, oil refineries, mining industries, textile industries, and paper industries. From these, the corporations dedicated to mining, textile, and leather tanning are the biggest generators of wastewater with toxic metals presence<sup>33</sup>, being lead (Pb), chromium (Cr), cadmium (Cd), copper (Cu) and nickel (Ni) the most abundant in their residual water because they are mainly used in the production of textile dyes<sup>34</sup>. These metal ions can reach human consumption through a distribution network that starts with the negligence of the industries at not applying an appropriate treatment to the wastewater generated by their activities before their final disposal<sup>33</sup>. These harmful compounds then reaches the fields ending in the soil, where they can filtrate till they make contact with groundwater, water that is used in agriculture activities, polluting food and in this way entering the human organism<sup>35</sup>.

Once toxic metals ions enter the human organism by food consumption, it could be absorbed by the digestive tract, then entering in body tissues and altering the appropriate function of the cells and their metabolism, implying a damage of the organs<sup>34</sup>. Evidently, the severity with which these metals can affect human health depends on the concentration consumed, however, the bioaccumulation of small traces of toxic metals can cause as dangerous consequences as high concentrations long term<sup>18,35</sup>.

This work is focus in chromium, which is considered a high-risk element by the Environmental Protection Agency (EPA) in the list of Public Health Statements about hazardous substances and their health effects. How chromium would affect the human organism depends on the time of exposure, concentration of the metal, its chemical nature – if it is Cr(III) or Cr(VI) – and how it enters the body<sup>36</sup>. The bioaccumulation of Cr(VI) in the human body can trigger stomach ulcers, anemia, affections in the male reproductive system by damaging the sperm, and it is even considered as a cancerogenic agent. Reports have shown an increase in lung cancer when people are exposed to inhalation of Cr(VI) as well as the fact that its ingestion can result in higher possibilities to develop stomach cancer<sup>37</sup>.

For this reason, in Ecuador regulations are set in place to control the maximum concentration of these potentially toxic metals allowed in freshwater and water for human consumption and domestic use. These regulations are: *Norma de Calidad Ambiental y de Descarga de Efluentes: Recurso Agua*<sup>38</sup> and the *Texto Unificado de Legislación Secundaria del Medio Ambiente (TULSMA)*<sup>39</sup>, and the permissible limits for metal concentrations set are presented in Table 2.1.

Table 2.1 Permissible Limit for metal concentrations in freshwater and water for human consumption and domestic use.  
 Extracted from Norma de Calidad Ambiental y de Descarga de Efluentes: Recurso Agua<sup>46</sup>.

Parameters	Chem Symbol	Units	Maximum Permissible Limit		
			Cold freshwater	Warm freshwater	Water for human consumption
Aluminum	Al	mg/L	0.1	0.1	0.2
Cadmium	Cd	mg/L	0.001	0.001	0.01
Chromium	Cr	mg/L	0.05	0.05	0.05
Cobalt	Co	mg/L	0.2	0.2	-
Copper	Cu	mg/L	0.02	0.02	1.00
Iron	Fe	mg/L	0.3	0.3	1.0
Lead	Pb	mg/L			0.05
Mercury	Hg	mg/L	0.0002	0.0002	0.002
Nickel	Ni	mg/L	0.025	0.025	-
Silver	Ag	mg/L	0.01	0.01	0.05
Zinc	Zn	mg/L	0.18	0.18	5.00

The importance of accomplishing the established limits has made necessary the application of different methods for removing metal ions from wastewater, the most common are chemical precipitation and ion exchange. Nevertheless, these methods lose their efficiency at low concentrations (1-100 mg/L), requiring greater use of resources<sup>20</sup> raising the treatment cost to counterproductive levels. Therefore, the need of bio-adsorbents is increasing every day, because of their high availability, low cost, high efficiency at low concentrations and low environmental impact<sup>18</sup>. For this reason, the *Moringa oleifera* and montmorillonite clay's properties are exploited in the pursuit of an effective and convenient bio-adsorbent.

# Chapter 3

## Objectives

### 3.1 General objective

Synthesis and characterization of composites consisting of *Moringa oleifera* seeds fiber extract along with natural Ecuadorian montmorillonite clay to be used in Cr(VI) removal from aqueous solutions through adsorption processes.

### 3.2 Specific objectives

These objectives were determined for a suitable fulfilment of the general objective.

- Synthesize composites from concentrated and activated montmorillonite clay and isolated organic solution from *Moringa oleifera* seeds fiber.
- Characterize the composites synthesized using FT-IR, DRX, SEM, XPS and EDX techniques to evaluate the correct binding between clay – *Moringa oleifera* seed.
- Evaluate the adsorption capacity of composites synthesized to determine the optimal performance conditions in the adsorption process.
- Estimate the most suitable isotherm of adsorption model that best fits with the experimental adsorption data.

# Chapter 4

## Theoretical Background

### 4.1 Adsorption

Adsorption is a spontaneous surface process that involves two species, one called adsorbent (commonly a solid and rarely a liquid) on whose surface is adhered the adsorbate (gases or dissolved substances), hence, the adsorption process depends on the affinity between adsorbate and adsorbent<sup>31</sup>. It is important to differentiate it from absorption, in which the adsorbate diffuses in the structure of the adsorbent<sup>40</sup>.

There are two types of adsorption, physical adsorption, also known as physisorption, and chemical adsorption also called chemisorption. The main difference between them is the change in enthalpy that each one causes<sup>41</sup>. Physisorption is when the molecules of the adsorbate stick to the adsorbent surface due to physical forces, mainly influenced by van der Waals interactions and weak attractive forces between adsorbate and adsorbent<sup>40</sup>. The change in enthalpy during physisorption is very low because the adsorbate molecules reach the adsorbent surface with low energy; which can be dissipated as heat and the adhesion to the surface is accomplished without any chemical change, bond formation or change in the energy state. For this reason, physisorption can be considered a very simple process to reverse<sup>41</sup>. On the other hand, chemisorption occurs when there is a chemical interaction between the molecules of the adsorbate and the adsorbent, commonly, a covalent bond is formed between them and it is specific for each type of adsorbate and surface<sup>40</sup>. In this case, the change in enthalpy is very high, and normally it requires an activation energy to ensure the adsorbate has the energy necessary to pass the energetic barrier for the chemisorption to occur<sup>41</sup>.

### 4.2 Adsorption Models

For an accurate comprehension of the adsorption systems is primordial to considerer the physicochemical condition of adsorption equilibrium<sup>42,43</sup>. Isotherms models are used for the

representation of a suitable adsorption mechanism, to know the adsorption capacity of the adsorbent, and allow to reveal the relation between the surface features of the adsorbent and the results obtained<sup>44,45</sup>. Nowadays there are several isotherms models that can describe the adsorption process, but the most frequently used are Langmuir, Freundlich, Dubinin-Radushkevich, and Temkin<sup>18</sup>. These models describe how the adsorption occurs on the surface of the adsorbent, the capacity of the adsorbent at different equilibrium concentrations and equilibrium relations, useful information for improving the adsorption system<sup>43,46</sup>. Langmuir and Freundlich models are two-parameter isotherm models that better fit in the metal adsorption processes<sup>45</sup>.

#### 4.2.1 Langmuir Model

Despite this model being originally conceived to interpret gas-solid phase adsorption, it is frequently the most accurate to predict metal adsorption process in raw water<sup>18,44</sup>. This model describes a monolayer adsorption in different adsorption sites of the surface, i.e., each adsorption sites can adsorb just one atom or molecule and no further adsorption can occur in the same site if it already is occupied<sup>18,44,46</sup>. This model sustains that each molecule of the adsorbate adheres to specific sites on the surface, these sites are energetically equivalent and the molecules adsorbed do not interact between each other<sup>41</sup>. The Langmuir equation is:

$$q_e = \frac{q_{max}K_L C_e}{1 + K_L C_e} \quad (1)$$

where  $q_e$  is the quantity of metal ion adsorbed per mass unit of adsorbent at equilibrium (mg/g),  $q_{max}$  is the amount of adsorbate at complete monolayer coverage (mg/g),  $K_L$  is Langmuir constant related to equilibrium constant of adsorption process (mg/g) and  $C_e$  is the equilibrium concentration of metal ions in solution (mg/L)<sup>18,44</sup>. This equation can be linearized to obtain:

$$\frac{C_e}{q_e} = \frac{1}{q_{max}K_L} + \frac{C_e}{q_{max}} \quad (2)$$

## 4.2.2 Freundlich Model

This model is used to describe the adsorption process in cases in which the surface presents an energy heterogeneity and it is not restricted by monolayer capacity. It details the heterogeneity of the surface, exponential distribution of the active sites for adsorption and their energies<sup>18,42,44</sup>. Freundlich is an empirical model which introduces multilayer adsorption. Freundlich equation is expressed as:

$$q_e = K_F C_e^{1/n} \quad (3)$$

where  $q_e$  and  $C_e$  have the same meaning that in the Langmuir model,  $K_F$  is the Freundlich constant related to adsorption capacity (mg/g), and  $n$  is the heterogeneity factor related to adsorption strength<sup>44,46</sup>. Once linearized the Freundlich equation becomes:

$$\ln q_e = \ln K_F + \frac{1}{n} \ln C_e \quad (4)$$

## 4.2.3 BET Model

It is an extension of the Langmuir model, developed by Brunauer, Emmet, and Teller<sup>41</sup>, commonly used to determine the surface area of a sample by nitrogen adsorption, leaving behind the monolayer principle but using the multilayer concept to consider the physical phenomena occurring during the adsorption<sup>47</sup>. This model shares some assumptions with Langmuir model, that is, that the adsorbent surfaces is energetically homogeneous, that there is no interaction between the adsorbed molecules, and that the last adsorbed layer is in equilibrium, that is, the rate of adsorption and desorption are the same<sup>48</sup>. The BET equation is defined as:

$$q_e = \frac{N_T \cdot \kappa \cdot x}{(1 - x)[1 + (\kappa - 1)x]} \quad (5)$$

where  $q_e$  is the adsorbed volume of the gas,  $N_T$  is the adsorbed monolayer volume,  $x$  is the relation of the equilibrium gas pressure with respect to the saturation pressure, and  $\kappa$  is the BET constant associated with the strength of adsorption<sup>48</sup>. The experimentally obtained data can be

fitted to this equation, and the resulting curve represents the BET isotherm, which can be classified into six types, described in the Table 4.1, and graphically represented in the Figure 4.1.

Table 4.1 Types of adsorption isotherms for different materials<sup>49,50</sup>.

Isotherm	Type of Material	Layer Formation	Type of adsorption
Type I	Microporous (diameter less than 2 nm).	Monolayer.	Chemisorption.
Type II	Mesoporous or/and non-porous.	Monolayer followed by multilayer.	Chemisorption and physisorption.
Type III	Macropores or/and non-porous.	Monolayer.	No fast-initial adsorption.
Type IV	Mesoporous (diameter 2 nm – 50 nm).	Monolayer followed by multilayer.	Occurs capillary condensation.
Type V	Mesoporous.	-	Occurs pore condensation.
Type VI	Non-porous with uniform surface.	First layer with simultaneous second formation.	-

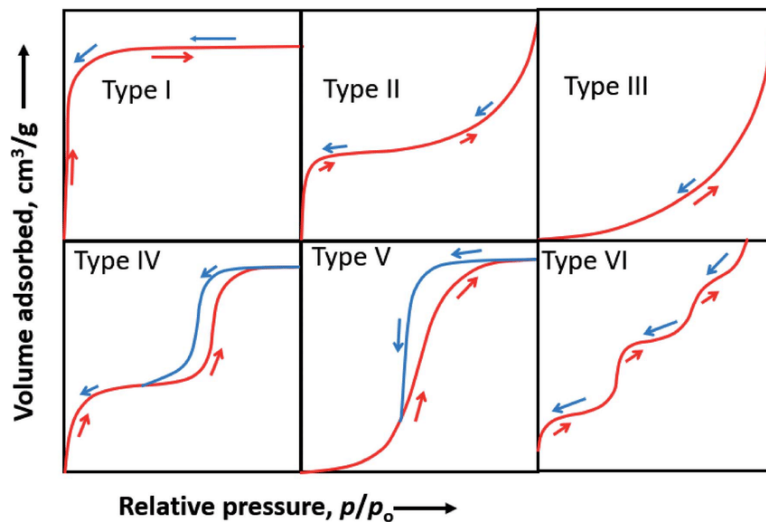


Figure 4.1 Graphic types of adsorption isotherms for different materials. Extracted from Aligizaki<sup>49</sup>

BET model was originally developed for gaseous phase adsorption and it is rarely used for the description of liquid phase adsorption processes<sup>51</sup>. In fact, in the classical for the BET equation, represented by equation 5, the term  $x$  corresponds to the ratio of the partial pressure of the adsorbate to its saturation partial pressure at the system temperature, that is  $x = P/P^s$ . However, have been reported some proposal to extend the BET model to liquid phase adsorption by some modifications in the analytical representation of the classical model<sup>52,53</sup>. One

of these suggests to replace the term  $x$ , described above, by  $x = C_{eq}/C_s$ , where partial pressure of the adsorbate ( $P$ ) is replaced by equilibrium concentration of adsorbate in liquid phase ( $C_{eq}$ ) and the saturation partial pressure ( $P^s$ ) is replaced by the saturation concentration of the adsorbate in liquid phase ( $C_s$ ), which is obtained from solubility data<sup>53</sup>. The problem with this assumption is that the BET isotherms, obtained in these cases, are very similar to Langmuir isotherms; even when it is not totally correct<sup>53</sup>.

Other proposals for modifying the classical BET model to be applied in liquid phase adsorptions result in the equation (6), which has three degrees of freedom, one more than for the classic model. These are  $q_e$ ; which has the same meaning as for the classic case (equation 5),  $K_{ML}$ ; representing the equilibrium constant of adsorption for the first layer, and  $K_{UL}$ ; which corresponds to the equilibrium constant of adsorption for upper layers. These modifications result in a better representation of the adsorption process implying the adsorbate in liquid phase on a solid surface of an adsorbent. The resulting equation for this modified BET model is represented by<sup>53</sup>:

$$q_e = \frac{N_T \cdot K_{ML} \cdot x}{(1 - K_{UL} \cdot x)[1 - (K_{UL} - K_{ML})x]} \quad (6)$$

### 4.3 *Moringa oleifera* in metal ions adsorption

*Moringa oleifera* is a bio-sorbent with the capacity for metals removal. In the case of bio-sorbents, during the adsorption process, the metal species are attracted by chemical sites found in the biomass being used as adsorbent, providing the possibility of recovering the metal ions and reusing the biosorbent<sup>18</sup>.

Metal ions adsorption can occur through different mechanisms such as complexation, physical adsorption, surface micro-precipitation, and ion – exchange, actually, more than one mechanism can happen at once, which of them depends on the functional groups on the surface of the adsorbent<sup>54</sup>. In the case of *Moringa oleifera*, being a lignocellulosic adsorbent<sup>18</sup> constituted primarily by cellulose, hemicellulose and, lignin the predominant mechanisms are ion – exchange or complexation<sup>42</sup>. The protein functional groups of the surface<sup>55</sup>, such as carboxylic

acid and amines, along with hydroxyl groups<sup>56</sup> make *M. oleifera* mostly an anionic polyelectrolyte leading to complexes formation with some metal ions in solution<sup>55</sup>.

Several conditions can alter the adsorption process, among the most influential variables are pH, temperature, contact time, metal ion concentration, and particle size of the adsorbent.<sup>57</sup> The pH of the solution is a very important factor to be considered, due to the acid-base interactions of the functional groups from the surface with metal species<sup>18</sup>. In the *M. oleifera* case, the presence of amino and acid groups causes their dissociation leading to interactions with metal ions depending on the pH<sup>42</sup>. *M. oleifera* adsorbent has an amphoteric character; hence, the pH value of the solution determines if its surface is positively or negatively charged<sup>18</sup>. It depends on the point of zero discharge ( $\text{pH}_{\text{pzc}}$ ), which in the case of *M. oleifera* seeds is between 6.0 and 7.0<sup>58</sup>; thus, the surface will have a positive, neutral or negative charge if  $\text{pH} < \text{pH}_{\text{pzc}}$ ,  $\text{pH} = \text{pH}_{\text{pzc}}$  or  $\text{pH} > \text{pH}_{\text{pzc}}$ , respectively<sup>18</sup>. Then, it is possible to modify the pH of the solution to increase the adsorption character of *M. oleifera* depending on if the metal is cationic or anionic.

#### 4.4 Montmorillonite clay in metal adsorption

Montmorillonite is a 2:1 type clay, which has two tetrahedral sheets with one octahedral sheet in the middle. In this octahedral sheet the isomorphous substitution of  $\text{Al}^{3+}$  by  $\text{Mg}^{2+}$  occurs, for this reason, it has a negative surface net charge, which makes it a great adsorbent for metal cations. Besides, montmorillonite clay has a layer charge density between 0.2 – 0.6 per half unit cell, resulting in a good layer expansion capacity. Both properties make of montmorillonite clay a great candidate for adsorption processes, without counting their low cost and environmentally friendly character<sup>59</sup>.

#### 4.5 Clay concentration

The montmorillonite clay used in this work comes from a natural source, for this reason, it is necessary remove all impurities and fractions such as: quartz, feldspar, cristobalite, etc. Hence, a pre-treatment is required before the composites are synthesized.

### 4.5.1 Carbonates removal

The presence of carbonates, especially of magnesium or calcium, can provoke soil segregation, decreasing the dispersion of the particles of clay, hindering the separation of the clay fraction. To remove the carbonates from the sample clay has been proposed an acidification process, however, the use of strong inorganic acids as hydrochloric acid or nitric acid can destroy the structure of clay. Hence, sodium acetate<sup>60</sup> is a better option because it reacts with the carbonates forming sodium carbonate, which is water-soluble, so it can be discarded in the supernatant in every wash performed on the clay. One of the proposed method to ensure the complete removal of carbonates, imply testing of the supernatant with barium chloride<sup>60</sup>, due to its capacity to react with carbonates, forming the water insoluble barium carbonate.

On the other hand, the presence of chlorides can affect the purity of clays, for which silver nitrate is recommended to be used<sup>60</sup>, due to the formation of silver chloride, an almost water insoluble salt. The white coloration of supernatant after silver nitrate addition is indicative of the chloride presence.

# Chapter 5

## Methodology

### 5.1 Materials and Chemical Reagents

Natural montmorillonite clay was extracted from the Guayllabamba Valley in the province of Pichincha, Ecuador and *Moringa oleifera* seeds were obtained from Guayaquil city in the province of Guayas. Chemical reagents used, such as sodium acetate, barium chloride, hydrogen peroxide, sodium hexametaphosphate, sulfuric acid, sodium chloride, silver nitrate, chloroform, methanol, potassium bromide, potassium chromate, nitric acid, and sodium hydroxide were acquired from Sigma Aldrich and Lobachem.

### 5.2 Activated Na-montmorillonite clay preparation

#### 5.2.1 Concentration of the montmorillonite clay

The concentration of montmorillonite clay treatment was based on the use of sodium acetate, hydrogen peroxide, and sodium hexametaphosphate, as has it been previously suggested by Flores and Alcalá<sup>60</sup>. Since the clay was naturally extracted from the Guayllabamba valley, it could contain montmorillonite, mica, kaolinite, quartz, feldspars, and other, for which was required the separation of the clay fraction from the soil samples. The procedure followed was as described below:

1. Raw material removal: For this, the soil sample was suspended in 2 L of distilled water inside a 2 L test tube, which was vigorously shaken and then let stand for 5 minutes. After that, only the clay fraction was collected by the pipette method.
2. Carbonates removal: It was mixed 385.87 g of natural clay with 4 L of distilled water, and 400 mL of a 1 M solution of sodium acetate at pH 5 was added. Then, the sample was centrifuged at 1500 rpm for 10 minutes to later discard the supernatant. This procedure was repeated twice more. The sample was then washed with 4 L of distilled

water twice till the supernatant was crystalline. The complete procedure was repeated three more times to ensure the total removal of carbonates. To check if the carbonates were completely removed, a few drops of concentrated barium chloride were added to the supernatant, any precipitate formation, or turbidity, was indicative of the presence of carbonates. In this case, this step was repeated until there were no traces of carbonates. Finally, the major quantity of distilled water was removed from the clay.

3. Organic matter removal: After ensuring complete carbonate removal, the sample was poured in a 2 L beaker and 25 mL of hydrogen peroxide 50% was added, generating high effervescence. After 10 minutes the effervescence had decreased, and the sample was heated at 60 °C till the effervescence stopped. This procedure was repeated three times more. The sample with the hydrogen peroxide was left to rest for 12 h till the reaction stopped and no more effervescence was generated. Then, the clay was dried at 90 °C for 24 hours and subsequently pulverized.
4. Final purification of clay: The pulverized clay sample was poured in a test tube with 2 L of water, and allowed to stand for 6 hours till equilibrium was reached. Then, 20 mL of sodium hexametaphosphate 5 g/L was added and vigorously agitated for 1 minute. The room temperature was recorded at ~ 24 °C, hence, according to Table 4.5.2 from the handbook of Flores and Alcalá<sup>57</sup>, the sample was allowed to stand for 7 hours and 28 minutes. After that, a fraction of the clay at 10 cm from the bottom of the test tube was removed with a pipette and dried at 40 °C for 24 h. The dried clay sample was triturated and weighed, resulting in a total mass of 187.33 g, the clay samples was stored for later use.

## 5.2.2 Montmorillonite acid activation

For the acid activation of the montmorillonite clay, concentrated sulfuric acid and concentrated barium chloride were used. This method of activation was based on the proposal of Bastardo et al<sup>61</sup>. To start the activation procedure, it was established an acid/clay mass ratio of 0.30. The procedure used is as follows:

In an Erlenmeyer flask, mix 100 mL of distilled water and 10 mL of sulfuric acid. Then, 50 g of montmorillonite clay was dispersed into the solution to form a suspension, which was

heated in a reflux system at 80 °C for 6 h with constant stirring. Once the reflux time had ended, the clay was recovered through gravity filtration and washed with 4 L of distilled water till all the sulphates present in the clay was removed. To ensure the complete removal of sulphates, concentrated barium chloride was added to the supernatant of each of the samples and then washed until no change was observed. Finally, the clay sample was dried at 90 °C for 24 hours, pulverized and stored for later use.

### 5.1.3 Ion exchange on the activated montmorillonite clay

For the ion exchange procedure was used sodium chloride and silver nitrate concentrated solutions, as has been suggested by Taffarel and Rubio<sup>62</sup>. The followed procedure is described below:

Using a proportion of 100 mL of sodium chloride 1 M solution for each gram of clay, add 45 g of activated montmorillonite clay was added in 4.5 L of a sodium chloride 1 M solution and stirred for 24 h. The clay sample resulting from the ion exchange treatment was washed with 4 L of distilled water three times until all the chlorides present in the supernatant is cleared away. For the absence of chlorides to be corroborated, no reaction should be observed in the supernatant by the addition of silver nitrate. Lastly, the activated Na-montmorillonite clay was dried at 90 °C for 24 h, pulverized and stored for the composite preparation.

## 5.3 Preparation of *Moringa oleifera* seed powder solution

### 5.3.1 Oil extraction from *Moringa oleifera* seeds

For the oil extraction from *Moringa oleifera* (MO) seeds, a mixture of chloroform, and methanol were used as extraction solvent. This procedure used is based on the proposal of Bhutada et al.<sup>63</sup>, which is described in the following with some modifications:

The shell-less MO seeds were soaked in distilled water for 4 h to clean up any possible dirt, and then they were dried at 40 °C for 24 h and pulverized to obtain the *Moringa oleifera* seed powder (MOSP). Then, 20 g of MOSP were collocated in a paper thimble, which was put in a Soxhlet glass tube and inserted in the extraction chamber of a Soxhlet apparatus. The extraction process

was carried out with 150 mL of a solvent mixture 2:1 of chloroform:methanol which was heated using a hot mantle. Once the whole system was ready, the Soxhlet extraction lasted 2 hours for a total of 10 refluxes, extracting all the oil contained within the MOSP. When the oil extraction finished, the de-oiled MOSP left in the paper thimble was left to dry at room temperature for 24 hours until the solvent was totally evaporated.

### 5.3.2 Extraction of de-oiled MOSP solution

For the development of this stage of the treatment, the procedure reported by Tukki et al<sup>64</sup> was followed: 1 g of MOSP was suspended in 20 mL of deionized water inside a polypropylene centrifuge tube. This tube was horizontally placed in a slow roller for 1 h until the extraction of the organic content of MOSP it was assumed complete. Then, the tube was placed vertically till the matter settled which facilitated the extraction of the supernatant. The resulting MOSP solution was stored for the composite preparation. This procedure was repeated two more times using 0.6 g and 0.2 g of MOSP, respectively.

## 5.4 Composite preparation

This procedure was based on the proposal of Tukki et al<sup>64</sup>. Here, 1 g of activated Na-montmorillonite clay was suspended in 5 mL of distilled water inside a polypropylene centrifuge tube, to which was added 10 mL of the supernatant of MOSP, previously prepared, and placed in the slow roller for 1 hour to allow the adsorption of the MOSP on the clay surface. Then, the tube was centrifuged for 5 minutes at 1200 rpm, and the supernatant and solid clay were separated, and then the clay was suspended in deionized water again. The centrifugation and washing with deionized water steps were repeated two times more to remove excess oxygen demand from the suspension. The whole procedure was repeated with different amounts of *Moringa* fiber incorporated to 1.0 g of clay, that is, 1.0 g, 0.6 g and 0.2 g of MOSP supernatant to obtain three different composites with different proportions of MOSP. These samples were denoted by Comp-11, Comp-16 and Comp-12, respectively. Once the composites were obtained, they were dried in a dry room with a temperature of 16 °C and pulverized to store for further analysis.

## 5.5 Characterization of the samples

### 5.5.1 Fourier - Transform Infrared (FTIR) Spectroscopy Analysis

FTIR analysis was used to determine the functional groups present in the activated Na-montmorillonite clay (AMN), *Moringa oleifera* seed powder (MOSP), and three composites samples (Comp-11, Comp-16 and Comp-12). This technique was carried out in the range of 4000–500  $\text{cm}^{-1}$ . For this, the samples were compacted with potassium bromide in a pastille that was placed in the spectrophotometer to measure.

### 5.5.2 Scanning Electron Microscopy (SEM) and Energy Dispersive X-Ray Spectroscopy (EDX) Analysis

SEM analysis was carried out to observe the surface morphology of samples. For this, a small amount of each sample was placed in a sample holder, on a piece of carbon tape. Then the samples were observed with a voltage of 20 kV and resolutions of 5000x and 8000x.

EDX analysis could be coupled with SEM for each sample chemical composition determination, that is, the elemental composition of each of them.

### 5.5.3 X-ray Diffraction (XRD) Analysis

XRD measures were done to qualitatively and quantitatively analyze prepared samples to obtain information on structures, phases, and crystal orientation, as well as other structural parameters phases present in the samples. For these analyses, the samples were pulverized until a very fine powder was obtained, which were subsequently placed in a sample holder to make the respective measurements.

### 5.5.4 X-ray Photoemission Spectroscopy (XPS) Analysis

XPS analysis was carried out to obtain the chemical composition from the sample surfaces and to analyze the possible reactions occurring between surface functional groups and evaluated adsorbents. For this, a small amount of each sample was placed in a sample holder, on a piece of carbon tape.

### 5.5.5 Surface Analysis

For these analyses some conventional techniques through the nitrogen gas adsorption were applied. Then using BET theory, variations in surface features, such as specific surface area and pore volume, of all the prepared composites were evaluated. The equipment used for the respective analyses was an AutoChem II 2920 from Micromeritics, an automated catalyst characterization system.

## 5.6 Adsorption Capacity Evaluation

Adsorption analyses were carried out to assess the ability (or capacity) of activated clay, *Moringa* fiber and prepared composites samples to remove potentially toxic metals from aqueous solutions. Given that the most important industrial activities in the Province of Imbabura involve chromium-based chemical species, potassium chromate was chosen as test metal ion, because it contributes to environmental pollution local. For the evaluation of the adsorption capacity, the quantification of chromium in solution before and after the adsorption processes was required, for which different spectrometric methods were used. The most common and reachable method, given the laboratory conditions, is based on the use of UV-Vis absorption spectroscopy, from which the concentration of dichromate ions was directly determined, and then it was related to the chromate ions concentration. (More details in Section 5.6.1).

Different experiments were developed to evaluate the effect of some variables on the adsorption process, such as the pH of the medium and time of contact between adsorbate and adsorbent. Below is a description of the three-stage procedure followed: in the first stage, a calibration curve was obtained by measuring the absorbance of each one of the solutions within a range of appropriate concentrations, according to the detection limits of the method. In the second stage, the most suitable experimental parameters to evaluate the efficiency of the prepared samples and composites for adsorption of Cr(VI) from aqueous solutions were determined. In the third and last stage, the adsorption capacity of each composite under convenient chosen conditions was assessed.

### 5.6.1 Calibration Curve Construction

Before starting the main procedure for the evaluation of chromium adsorption capacity, it was necessary to estimate the concentration range of solutions to be analyzed, and from these values, the calibration curve was constructed. For this, a stock solution of potassium chromate was prepared by dissolving of 0.93 g of potassium chromate in 250 mL of distilled water, using a volumetric flask. From this stock solution, six solutions with concentrations of 100 ppm, 200 ppm, 300 ppm, 400 ppm, 500 ppm, and 600 ppm in Cr(VI), respectively, were prepared. To each solution, few drops of nitric acid were added to form dichromate ion from chromate ion in solution, which allowed to record the absorbance measurements using a UV-Vis spectrometer. The absorbance was recorded at a wavelength of 444 nm, and from the absorbance measurements of each of the solutions tested, the calibration curve was constructed based on the Lambert-Beer Law.

### 5.6.2 Determination of suitable parameters

To determine the most convenient parameters to evaluate the Cr(VI) adsorption process on the prepared composites, first, tests under the extreme parameters of concentration of the metal ion, pH of solutions, and contact time were carried out. In all cases a proportion  $m_{\text{adsorbent}} : V_{\text{Cr-solution}}$  given by 10 g : 1 L was used.

To start, 100 mL of a stock solution of 3000 ppm was prepared by dissolving 1.12 g of potassium chromate in distilled water inside a volumetric flask. From this solution, four additional solutions were prepared, which corresponded to:

- Two solutions of 100 ppm, one of them with pH = 2 and the other with pH = 9.
- Two solutions of 600 ppm, one of them with pH = 2 and the other with pH = 9.

For the 100 ppm chromium solutions, 3.33 mL of the potassium chromate 3000 ppm solution were diluted with distilled water in a 100 mL volumetric flask. In one of these solutions, a few drops of nitric acid were added until a pH = 2 was reached, while in the other solution a few drops of sodium hydroxide were added until a pH = 9 was reached. For the 600 ppm

chromium solutions, it followed a similar same procedure, but in this case, 20 mL of the potassium chromate 3000 ppm stock solution were diluted to 100 mL with distilled water.

Once all solutions were prepared, the adsorption analysis started by mixing 0.08 g of Comp-11 in 8.0 mL of the acid solution of potassium chromate 100 ppm. This sample was stirred for 1 hour in a magnetic plate, and then it was filtered by gravity. The absorbance at 440 nm was recorded for the resulting solution, using a UV-Vis spectrometer. This analysis was also carried out for activated Na-montmorillonite, MOSP, and Comp-16 and Comp-12 samples.

Then, 0.08 g of Comp-11 was mixed with 8.0 mL of the 100 ppm potassium chromate basic solution, previously prepared. Same as the case described above, this sample was stirred for 1 hour, filtered by gravity and the absorbance at 444 nm was recorded using a UV-Vis spectrometer. This procedure was repeated for activated Na-montmorillonite, MOSP, Comp-16 and Comp-12 samples.

The whole process was repeated once more, but increasing the contact time between solid and solution for 17 hours, keeping the stirring, to then compare the different contact times tested and thus define the optimal experimental conditions for Cr(VI) adsorption.

### 5.6.3 Variation of initial concentration Cr(VI) - Adsorption Isotherms

To start, a 1000 ppm stock solution was prepared by dissolving 0.93 g of potassium chromate in distilled water and poured in a 250 mL volumetric flask. From this solution, it was prepared six solutions more with concentrations of 100 ppm, 200 ppm, 300 ppm, 400 ppm, 500 ppm, and 600 ppm of chromium, respectively. All these solutions were prepared by adding nitric acid to reach an acid solution with  $\text{pH} = 2$ . Then, 0.08 g of activated Na-montmorillonite was suspended in 8.0 mL of the 100 ppm chromium solution. With help of a magnetic plate, this sample was stirred for 3 hours, then it was filtered by gravity and finally, the absorbance at 444 nm in a UV-Vis spectrometer was recorded to determine the difference in chromium concentrations, before and after the adsorption process. This procedure was repeated with the same adsorbent by changing the chromium concentration of the solutions for 200 ppm, 300 ppm, 400 ppm, 500 ppm, and 600 ppm. Subsequently, the other different prepared adsorbent, such as

MOSP, Comp-11, Comp-16, and Comp-12 replaced the activated Na-montmorillonite, and the same procedure, with all chromium solutions, was carried out.

# Chapter 6

## Results and Discussion

### 6.1 FT-IR Analysis

The FT-IR analysis was carried out to identify the functional groups in the montmorillonite, MOSP, and prepared composites, which would allow to determine which surface functional groups are responsible for the binding of Cr(VI) on the adsorbents. Also, from this analysis it is possible to evaluate the effect of the composite synthesis.

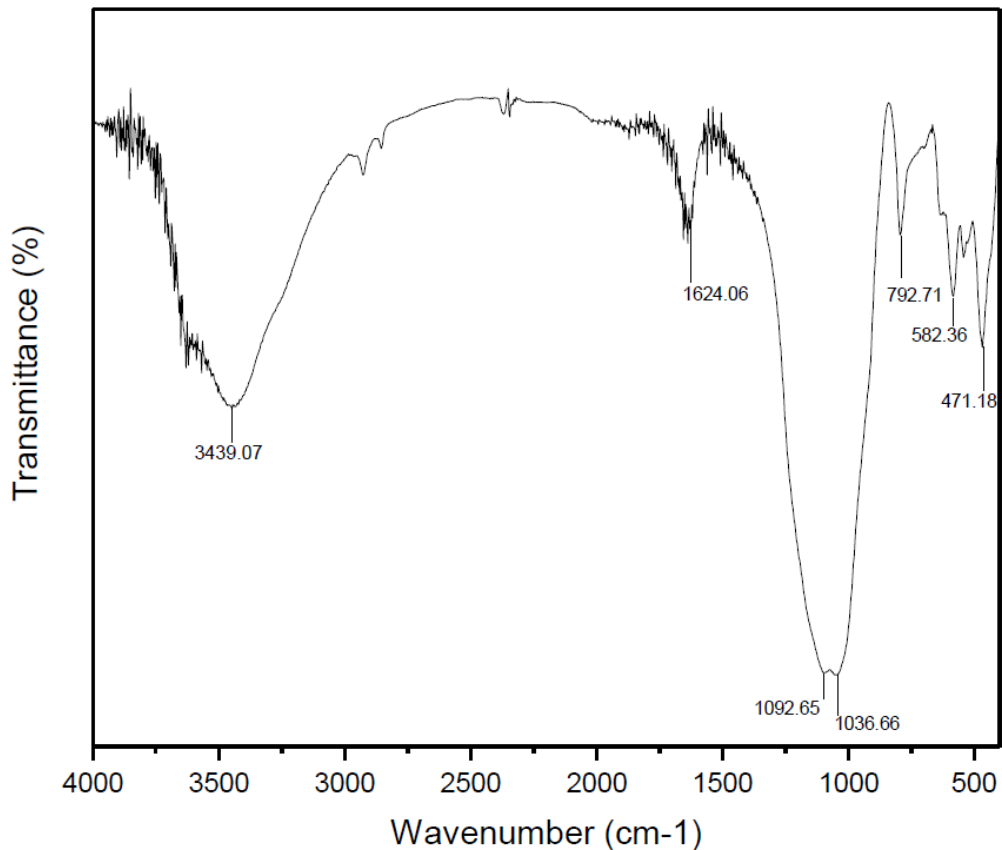


Figure 6.1 FT-IR spectrum of activated Na-montmorillonite

In the spectrum for montmorillonite shown in the Figure 6.1, the band at 3439.07 cm<sup>-1</sup> indicates the presence of the outer surface -OH stretching. The absorption band at 1624.06 cm<sup>-1</sup> represents the -OH bending vibration, while the band between 1092.65 cm<sup>-1</sup> and 1036.66 cm<sup>-1</sup>

shows the Si-O bending vibration and its stretching vibrations are observed at  $792.71\text{ cm}^{-1}$ . Also, the Al-O-Si skeletal vibrations are showed at  $582.36\text{ cm}^{-1}$  and  $471.18\text{ cm}^{-1}$ .<sup>65</sup> Figure 6.2 shows a comparison between spectra for the treated montmorillonite clay and the commercially acquired montmorillonite clay reagent. Both spectra share the peaks described above, confirming the high purity of the montmorillonite clay used for the composite's preparation.

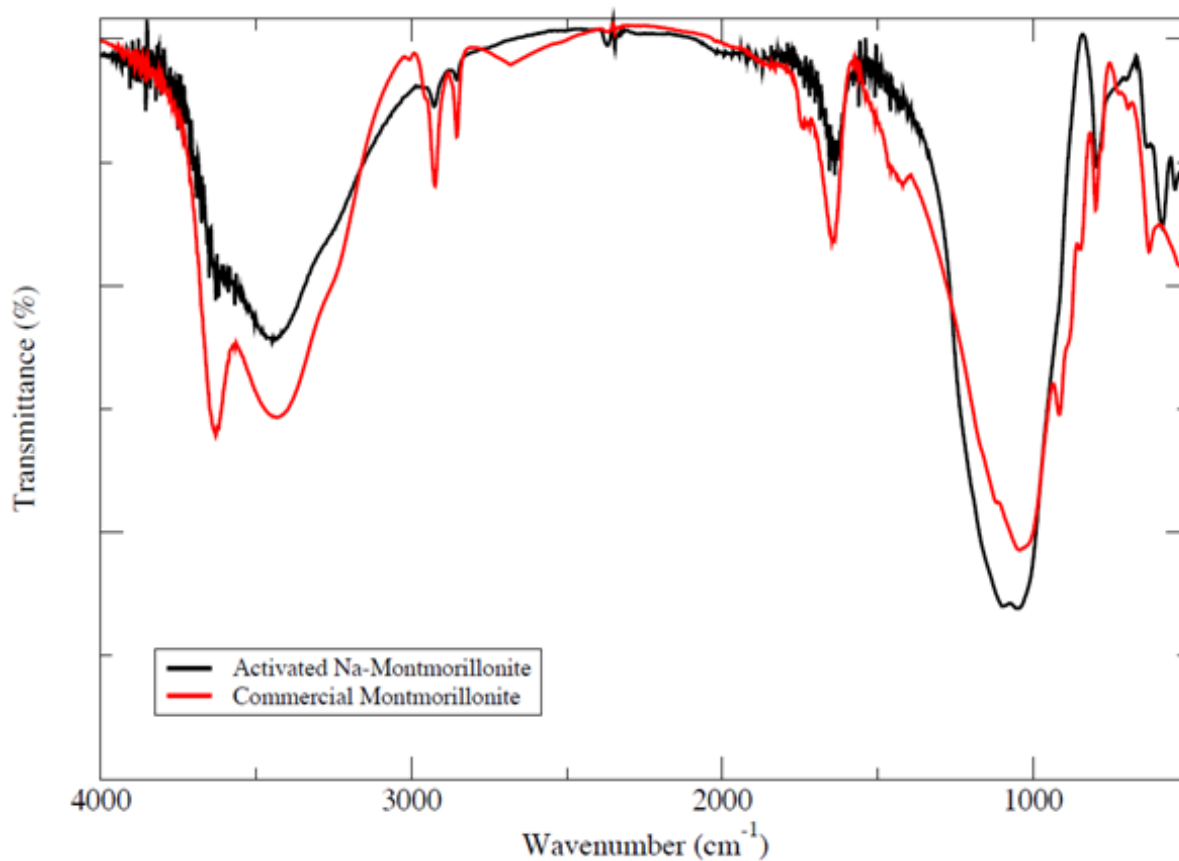


Figure 6.2 FT-IR spectra for activated Na-montmorillonite and commercial montmorillonite.

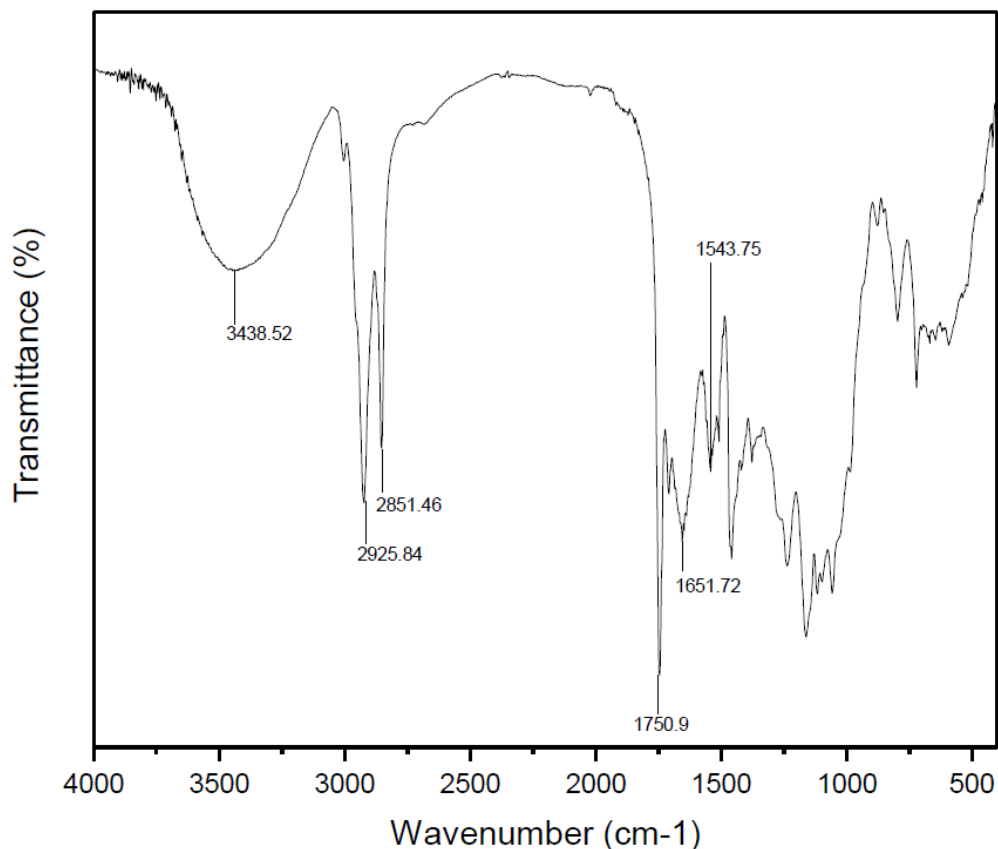


Figure 6.3 FT-IR spectrum of MOSP

In Figure 6.3 the FT-IR spectrum for MOSP is presented. A band can be observed at  $3438.52\text{ cm}^{-1}$  corresponding to the stretching of -OH bonds from the proteins, fatty acids, and carbohydrates units; for the high protein concentration in the seeds, this band is associated with a contribution from N-H stretching of the amide bond. The peaks at  $2925.84\text{ cm}^{-1}$  and  $2851.46\text{ cm}^{-1}$  are attributed to the C-H bond of the  $\text{CH}_2$  group, given the high intensity of these peaks, it can be associated with the lipid content remaining in the seed. At  $1750.9\text{ cm}^{-1}$  a peak is observed that could be related to the C=O stretching from the carbonyl group of the lipids, while the peak at  $1651.72\text{ cm}^{-1}$  is related to the carbonyl amides from the protein part. Finally, at  $1543.75\text{ cm}^{-1}$  is observed a peak that may be attributed to stretching  $\text{C}\equiv\text{N}$  and to the deformation of the N-H bond<sup>18</sup>.

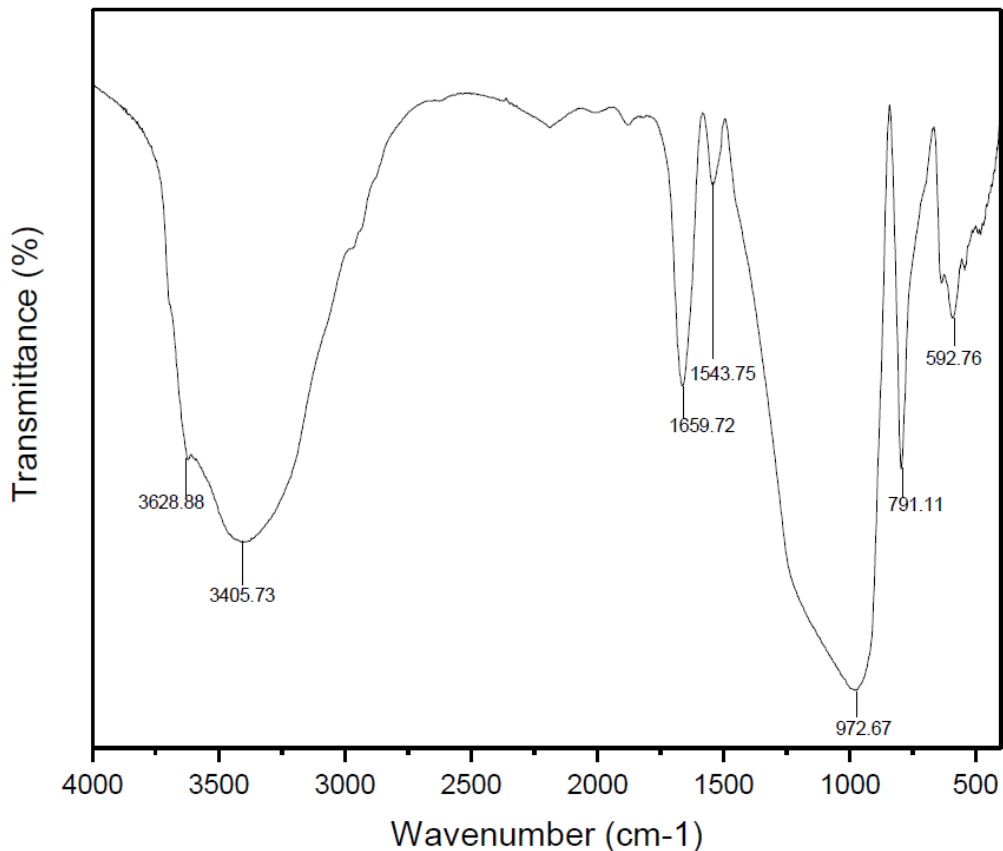


Figure 6.4 FT-IR spectrum of for the composite Comp-11

Figure 6.4 shows the spectrum for Comp-11 sample, in it can be observed the similarity with the spectrum of montmorillonite; this is to be expected because the clay is the principal matrix in the composite preparation. Therefore, the focus should be on identifying the representative peaks for MOSP. There is a broad band at 3405.73 cm<sup>-1</sup> attributed to the -OH stretching from clay and MOSP, however, a small peak appeared in the band at 3628.88 cm<sup>-1</sup>, which is related to an undertone of stretching of C=O group from protein part of the MOSP, confirming the formation of the composite. Similarly, at 1659.72 cm<sup>-1</sup> there is a peak attributed to the carbonyl amides from MOSP. At 1543.75 cm<sup>-1</sup> there is a peak that can be associated with stretching CN and to the deformation of the N-H bond from the proteins. At 972.67 cm<sup>-1</sup> there is an overlapped band related to the Si-O bending vibrations, while its stretching vibrations can be observed at 791.11 cm<sup>-1</sup>. The skeletal vibrations form Al-O-Si is located at 592.76 cm<sup>-1</sup> in the spectra<sup>18,65</sup>. These peaks are indicated in the Figure 6.4.

Spectra for other two composites Comp-16 and Comp-12 are shown in the Annex 1.

## 6.2 SEM and EDS Analysis

Figure 6.5 shows the SEM images for the Comp-11 (A) and the activated Na-montmorillonite (B). There is a remarkable difference between them with respect to their surface morphology. In fact, the compound micrograph in Figure 6.5-A suggests the presence of a dust-covered surface compared to the micrograph shown in Figure 6.5-B, in which the morphology of the structure is better defined, that is, suggesting a cleaner surface. This can be due to the presence of MOSP in the composite (Figure 6.5-A), that is not present on the clay (Figure 6.5-B). Both images show the irregular and porous surface of the clay. Due to the resolution (5000x) it was not possible to evaluate the inner conformation of the sample, but a crystalline structure and stacking of sheets can be observed, which is consistent with previous report in the literature<sup>66</sup>.

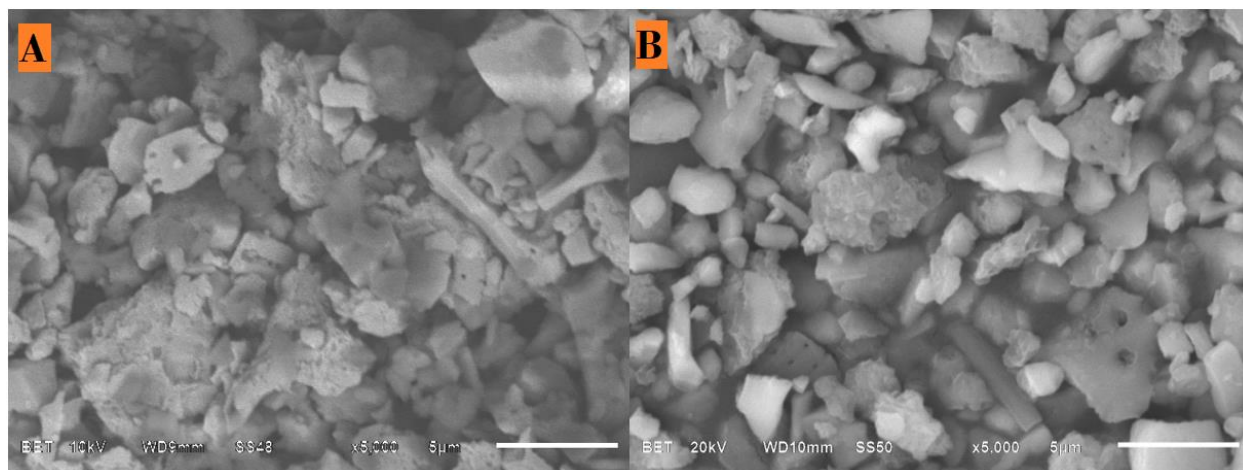


Figure 6.5 SEM images A. Composite 1.1 and B. Activated Na-montmorillonite.

SEM images can prove the presence of MOSP in the composites; thus, elemental analysis was done to verify any change in the composition of the clay. Table 6.1 shows the chemical composition of the evaluated materials, indicating a high content of silicon and the lack of carbon in activated Na-montmorillonite (AMN). For the MOSP case high levels of carbon is observed which is consistent with the *Moringa* seeds composition. With respect to the composites the presence of silicon and carbon suggests that MOSP was adsorbed on the surface of the AMN clay during the formation process of composites.

Table 6.1 Chemical composition of the surfaces of Activated Na-montmorillonite (AMN), MOSP, Comp-11, Comp-16 and Comp-12 analyzed by EDX.

Samples	Elements present in the samples (%)						
	Oxygen	Sodium	Aluminum	Silicon	Potassium	Iron	Carbon
AMN	54.77	2.22	6.80	31.15	1.35	2.30	-
MOSP	32.38	-	-	-	1.24	-	67.36
Comp-11	53.28	1.48	5.30	24.12	1.13	1.45	32.07
Comp-.6	49.73	0.96	2.89	12.24	0.52	0.62	32.67
Comp-12	51.17	1.09	2.77	11.83	0.47	0.56	31.74

### 6.3 XRD Analysis

The obtained XRD diffractograms confirm the nature and phases present in the clay sample (AMN) and the composites prepared from it. To ensure the nature of the clay, the diffractogram of montmorillonite extracted from a mineral database was used to compare it with the diffractogram obtained from the clay sample prepared.

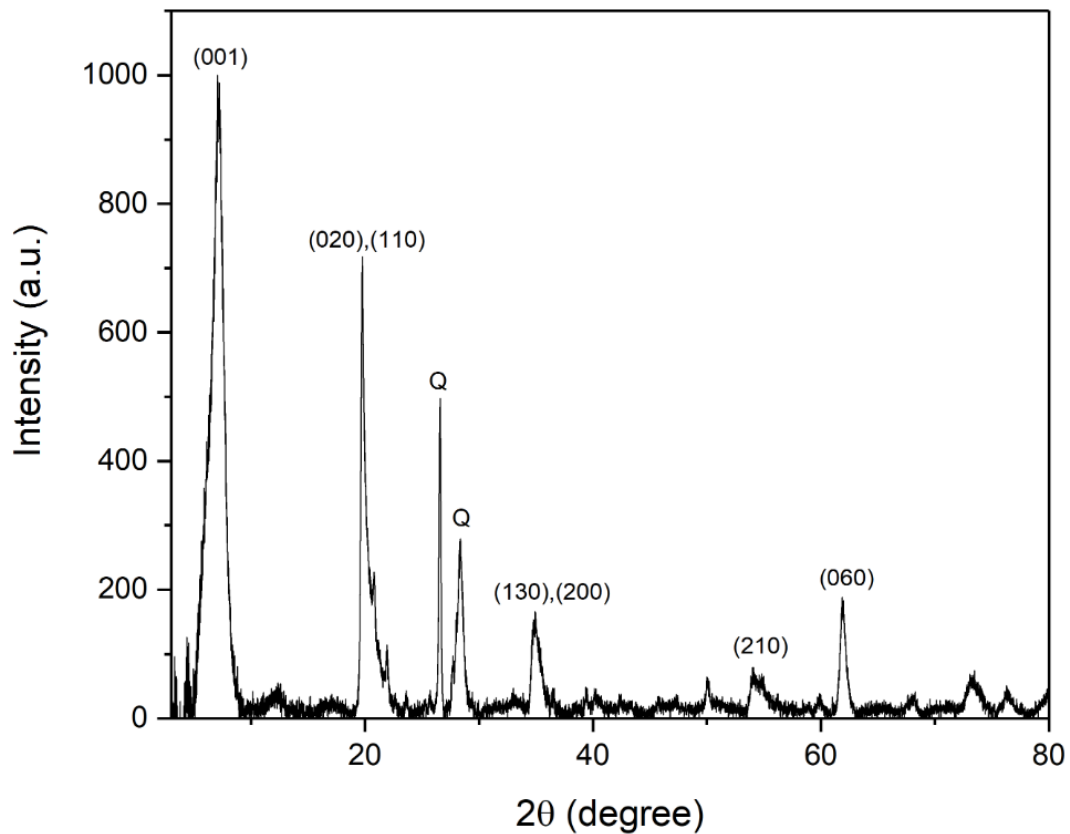


Figure 6.6 XRD diffractogram for activated Na-montmorillonite

Figure 6.6 shows the XRD diffractograms for activated Na-montmorillonite extracted from Guayllabamba – Ecuador and concentrated. The characteristic diffraction in the plane (001) at  $7.049^\circ/2\theta$  with a corresponding basal spacing of  $12.53 \text{ \AA}$  can be observed. Normally, this plane should be localized around  $6^\circ/2\theta$  with a  $d = 15 \text{ \AA}$ , however, the value can vary according to the hydration of the montmorillonite, in this case, activated Na-montmorillonite is dehydrated, which shifts  $2\theta$  to a higher value<sup>67</sup>. Another important diffraction plane is (060), which indicates the dioctahedral structure of the clay<sup>68</sup>, this diffraction plane is found in  $61.97^\circ/2\theta$  with a basal spacing of  $1.50 \text{ \AA}$ . The other diffraction planes (020), (110), (130), (200), and (210) are characteristic of type 2:1 clay, confirming its nature. Nevertheless, between  $26^\circ/2\theta$  and  $28^\circ/2\theta$  bands corresponding to quartz are found in the sample. Furthermore, in Figure 6.6 the activated Na-montmorillonite diffractogram (Figure 6.7-B) with the XRD data for montmorillonite from a certified database<sup>69</sup> are compared (Figure 6.7-A), the similarity between patterns and the presence of the characteristics diffraction planes corroborate that the purified clay is, indeed, montmorillonite clay.

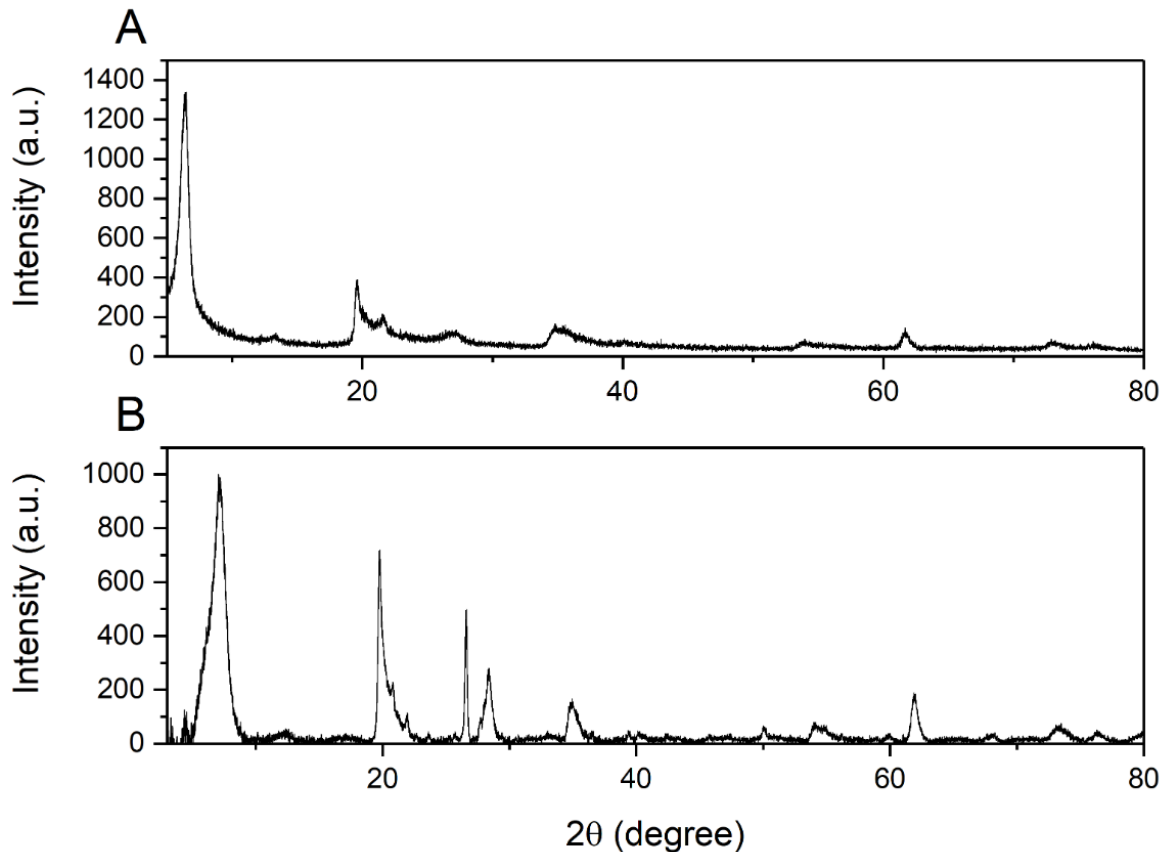


Figure 6.7 XRD diffractogram of A. Database montmorillonite and B. Activated Na-montmorillonite

In Figure 6.8 A the diffractogram for Composite 1.1 is shown, every peak found in Figure 6.6 is also showed in the diffractogram corresponding with Composite 1.1. The characteristic peaks of diffractogram planes (001) and (060) are at  $7.04^\circ/2\theta$  and  $61.97^\circ/2\theta$  respectively. So, as Figure 6.8 shows, no peak has shifted or changed their  $2\theta$  values. Hence, the basal space (d spacing) between planes have no changed for the presence of MOSP in the activated Na-montmorillonite clay, confirming that the composite is formed by the surface interaction between the clay and the MOSP but not for the sorption of the MOSP inside the structure of the clay.

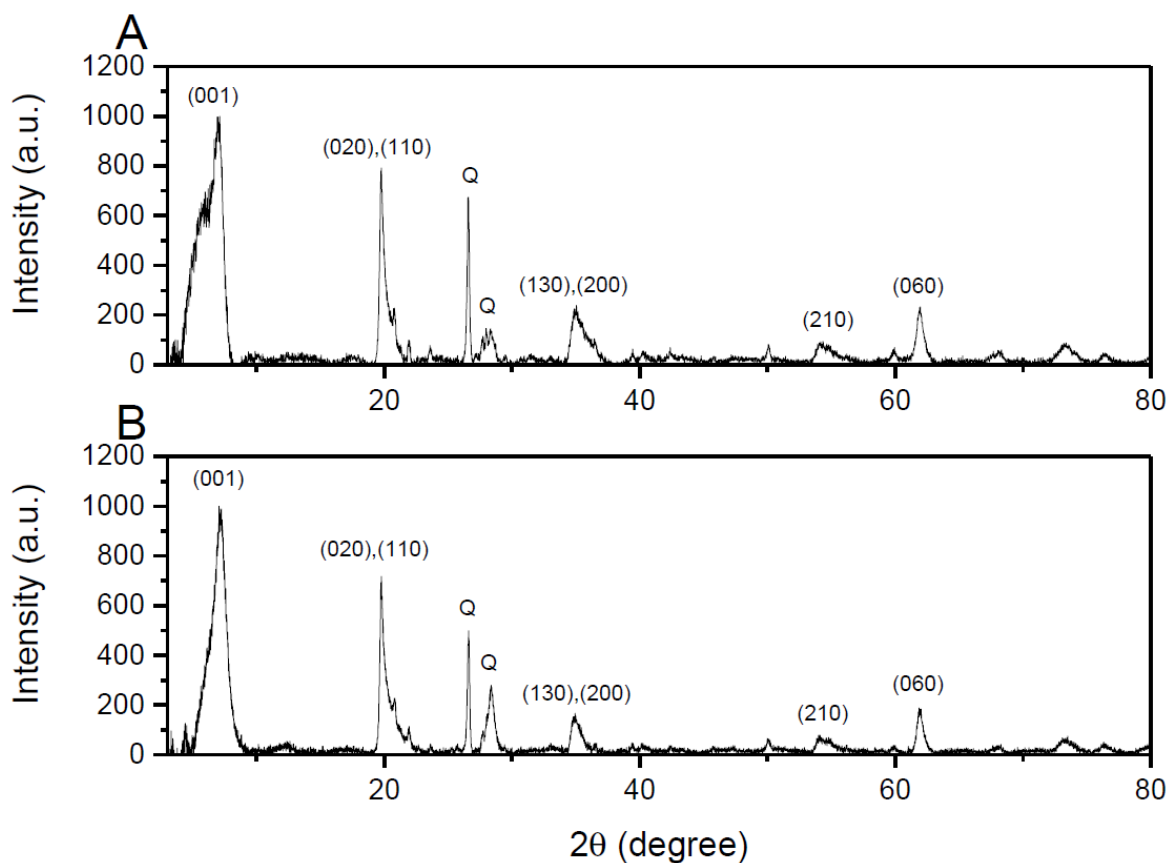


Figure 6.8 XRD diffractogram for A. Composite 1.1 and B. Activated Na-montmorillonite.

## 6.4 XPS Analysis

This analysis shows the surface chemical composition and the chemical state of the surface elements of the samples. In Figure 6.9, the complete spectrum, called survey spectrum, from activated Na-montmorillonite (AMN), Comp-16 (in the figure called COMP) and the composite after Cr(VI) adsorption (COMP Cr(VI)) are presented. It shows that the elements mainly found are aluminum (Al2p), silicon (Si2p), carbon (C1s), nitrogen (N1s), oxygen (O1s), iron (Fe2p) and sodium (Na1s). To analyze the chemical state of oxygen, carbon and nitrogen elements were separately evaluated the regions associated with them, and the corresponding results are shown in Figures 6-10, 6-11 and 6-12, respectively.

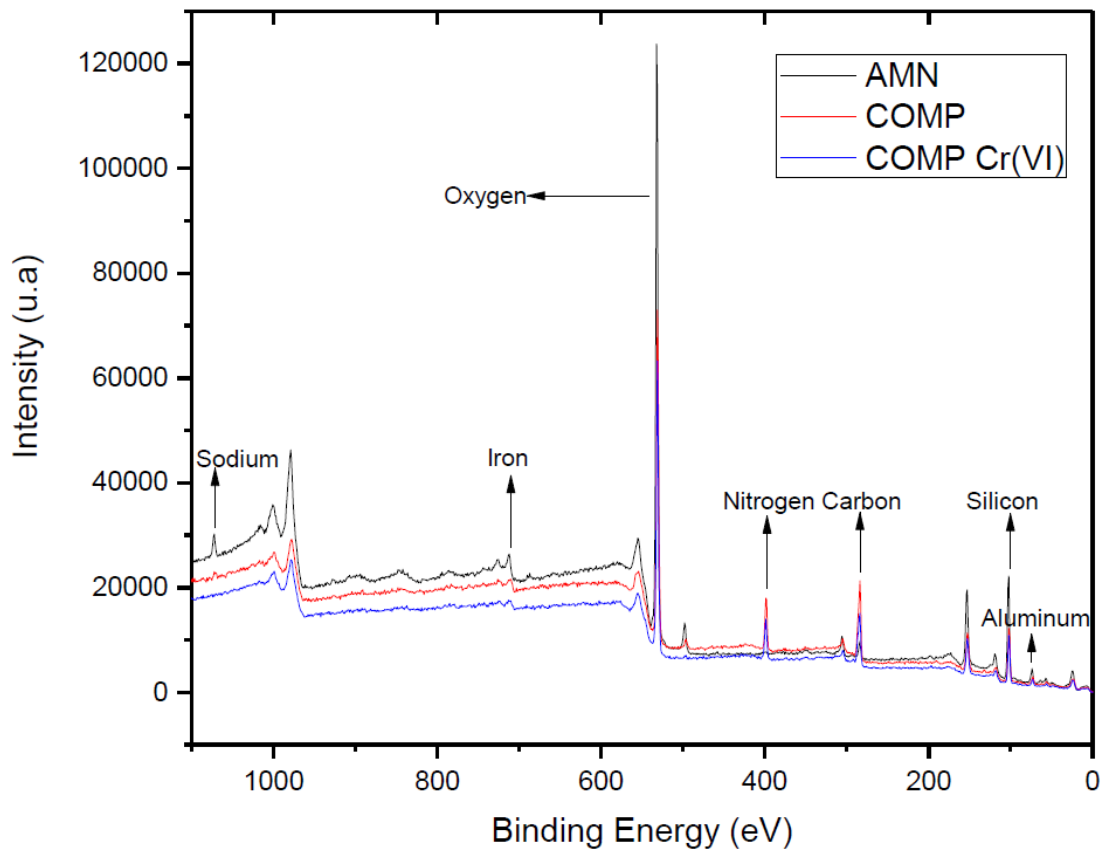


Figure 6.9 XPS pattern for activated Na-montmorillonite, Comp-16 and Composite with Cr(VI) adsorption.

In Figure 6.10 is represented the pattern for O1s, from it is easy to conclude that the concentration of oxygen in AMN is higher than in the composites. But the most important detail is the shift in binding energy of oxygen associated with the montmorillonite ( $\sim 532$  eV<sup>70</sup>) and for the case of functionalized-montmorillonite with MOSP, with a binding energy observed at 530.8 eV. It could be due to the occurrence of bonds between surface atoms of clay and the oxygen from the organic matter introduced with the MOSP. The bonds found could be associated with carbonyl groups, or even, carboxyl groups related to the protein content from the MOSP. While in the case of the composite after Cr(VI) adsorption, in addition to its notable reduction in concentration, its binding energy suffers another slight shift to higher binding energy ( $\sim 531.2$  eV). This may be due to the possible formation of Cr<sub>2</sub>O<sub>3</sub> during the adsorption of Cr(VI) on the surface of the composite<sup>70</sup>.

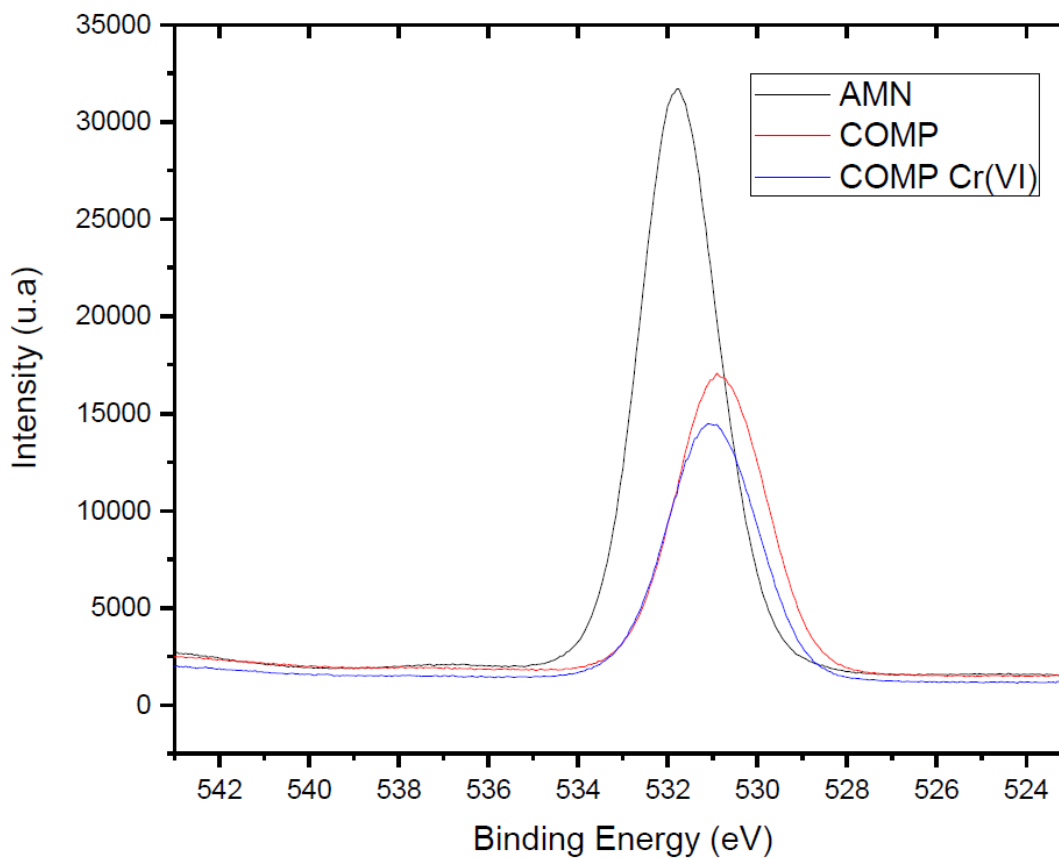


Figure 6.10 XPS pattern for Oxygen (O1s) for different samples evaluated

In Figure 6.11 the pattern for carbon (C1s) is shown. The presence of carbon band in AMN sample can be related with the fact of had used conductive carbon tape on sample holder. There is a remarkable increase in the concentration of carbon that is observed for the montmorillonite clay when it is functionalized with MOSP. Evidently, it is due to the increment of organic matter on the clay for the presence of MOSP adsorbed on the clay's surface. The main peak found in the three patterns is associated with C-H or C-C bonds<sup>71</sup>. The other peaks present in COMP (Comp-16) and COMP Cr(VI) are attributed to C=O and C-O bonds<sup>71</sup>, because MOSP presence contributes with carbonyl and carboxyl groups for its protein and fat content, respectively.

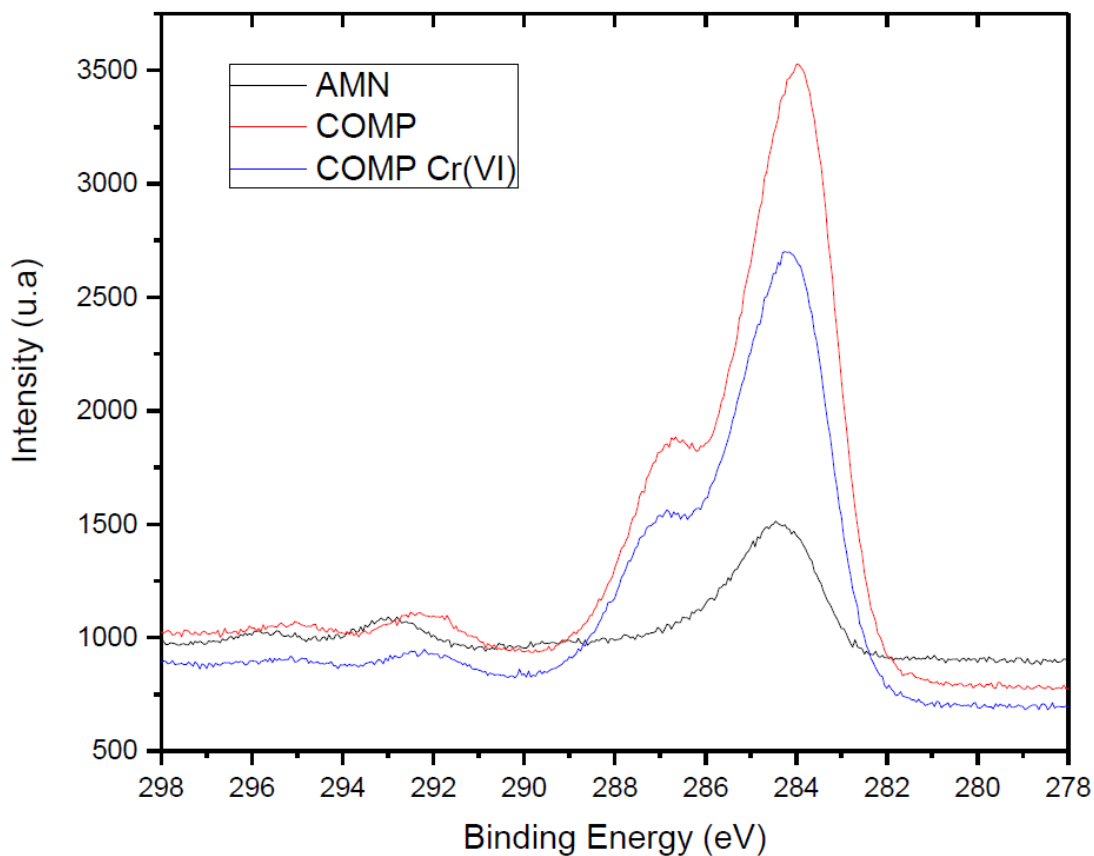


Figure 6.11 XPS pattern for Carbon (C1s)

In Figure 6.12 the spectra for nitrogen content in the samples is presented. The absence of nitrogen in montmorillonite clay is evident because there is no peak in its spectra. Nevertheless, for both composites, the concentration of nitrogen is increased due to the protein content from MOSP and their position around 398 eV demonstrates the presence of amines groups. Besides, in the patterns for COMP (Comp-16) and COMP Cr(VI) is observed a very slight shift in peak for nitrogen, this may be caused by the formation of other type of bond, for example, between nitrogen and chromium species, possibly  $\text{Cr}_2\text{N}$  or  $\text{CrN}$  bonds, whose binding energy has been reported to be found between 397 eV and 396 eV<sup>70</sup>. This assumption is possible for the adsorption of Cr(VI) in the surface of the composite.

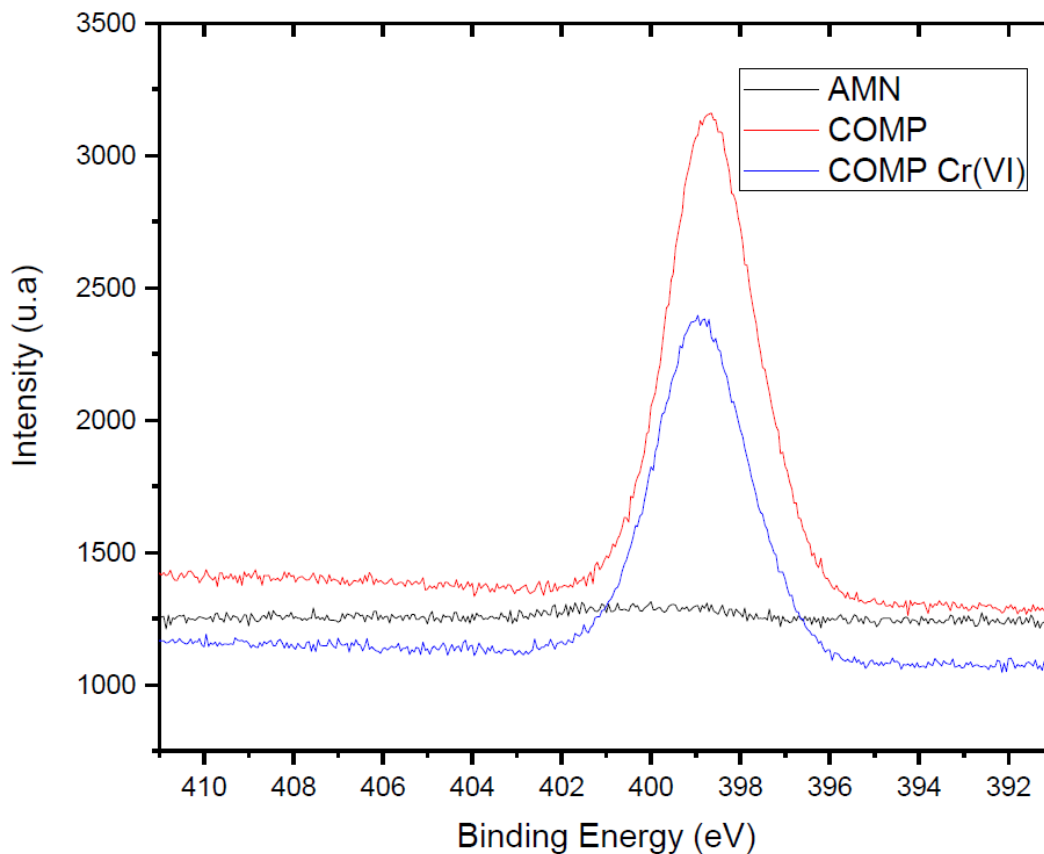


Figure 6.12 XPS pattern for Nitrogen (N1s)

Considering the presence of chromium species, mentioned above, was required to carried out a XPS analysis inside chromium region for the prepared samples to confirm it. In Figure X the XPS pattern for evaluate the chromium content is shown. At a glance, all the samples seem to be lacking of chromium, however, for the composite after of adsorption process (COMP Cr(VI)) shows a slight bulge at 576 eV. This small bulge can be related to Cr<sub>2p<sub>3/2</sub></sub> band, referring to chromium nitride resulting from the interaction between the Cr(VI) from the solution and nitrogen from the surface composite. To confirm this assumption is required to carry out further analysis using composites with a higher chromium concentration and a longer duration of XPS experiment<sup>70</sup>.

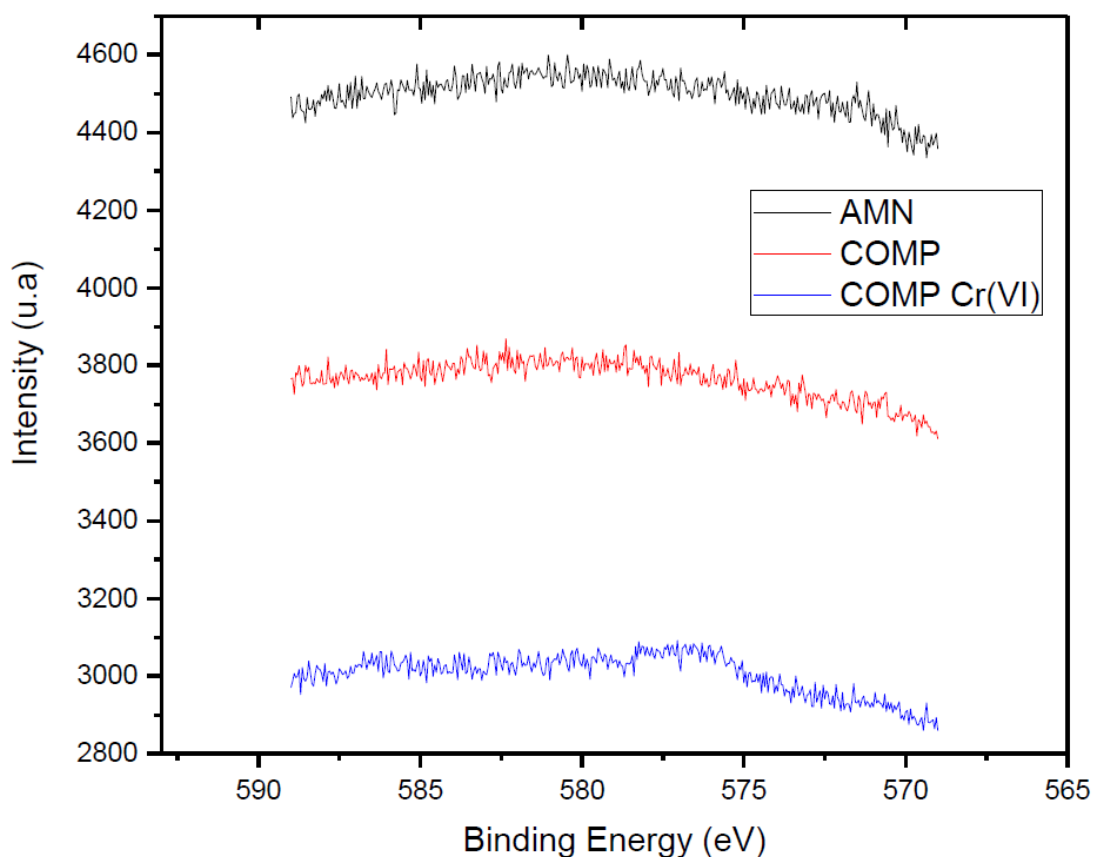


Figure 6.13 XPS pattern for Chromium (Cr<sub>2p<sub>3/2</sub></sub>)

## 6.5 Surface Area Analysis

The surface area, monolayer volume, and pore volume were obtained by experiments based on nitrogen adsorption on the samples and analyzed by BET theory. For this, an initial atmospheric pressure of 542 mmHg was used, which reaches the saturated pressure at 557 mmHg. From this analysis were obtained the values shown in Table 6.2.

*Table 6.2 BET surface areas from Nitrogen adsorption on AMN and functionalized composite.*

<b>Samples</b>	<b>Monolayer Volume (cm<sup>3</sup>/g)</b>	<b>BET Surface Area (m<sup>2</sup>/g)</b>	<b>Total Pore Volume (cm<sup>3</sup>/g)</b>
AMN	17.21	74.91	0.0376
Composite	3.98	17.31	0.0087

Data from Table 6.2 shows a notable decrease in the monolayer volume, BET surface area and total pore volume of the activated Na-montmorillonite when it was functionalized with MOSP to form the composites. It evidenced the molecules from MOSP adsorbed on the surface of the clay, which occupy some active sites and reduce the surface area of the clay. Despite this decrease of surface area, the presence of the MOSP molecules in the clay could change the chemical structure of the surface of the clay and would contribute to the chromium adsorption process. This chemical change is related to the functional groups incorporated by the MOSP presence.

## 6.6 Adsorption Analysis

To understand how Cr(VI) adsorption system works, it was necessary to interpret the interactions between the adsorbate (chromium ions) and the adsorbent (AMN, MOSP and Composites). In this case, parameters as contact time, pH, and initial Cr(VI) concentration were evaluated to carried out suitable adsorption processes.

To begin the complete analysis, a calibration curve for Cr(VI) was constructed to obtain the linear regression parameters from Lambert-Beer Law fit, and to get the Cr(VI) concentration of each solution sample. The Lambert-Beer Law sustains that the absorbance is directly proportional to the concentration<sup>72</sup>. The resulting equation as well as the R-coefficient is shown

in the inset of the Figure 6.14, and from this equation the chromium concentration of the analyzed solutions was estimated.

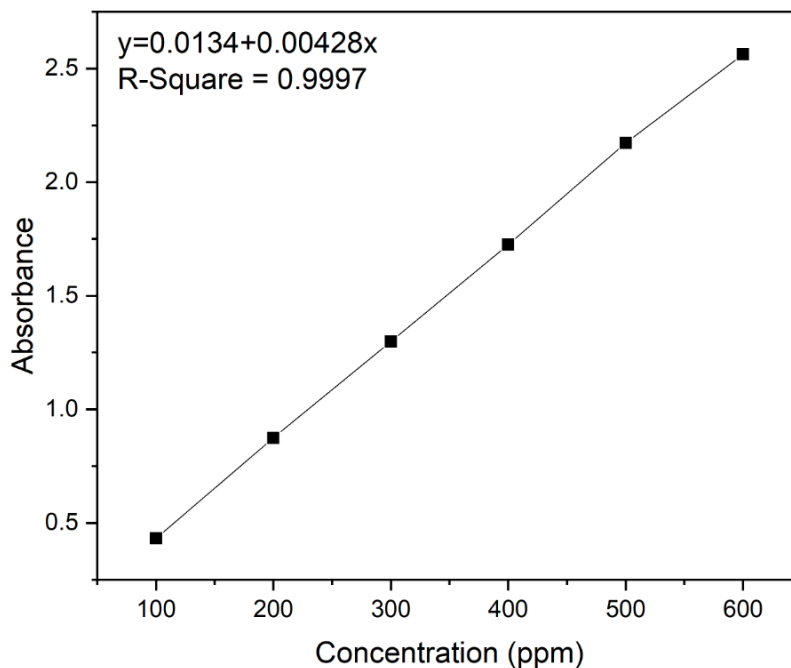


Figure 6.14 Calibration curve for Cr(VI)

### 6.6.1 Effect of the pH

In the adsorption process, the pH of medium is one of the most important parameters that can affect or modify the performance of the adsorbent, because it can alter the charge density on the adsorbent surface<sup>73</sup>. Besides that, it can control the degree of ionization of adsorbate in solution<sup>74</sup>. To evaluate the influence of pH on the adsorption of Cr(VI) ions, experiments at room temperature in which the pH of solutions were fixed were carried out, and the chosen values were 2 and 9, respectively. The initial concentration for Cr(VI) solution was fixed in 100 ppm and the adsorbent ratio; solution volume remained at 10 g/L, with two different contact times of 1 hour and 17 hours. The results presented in Figure 6.16 reveal that lower pH values show the highest percentage of removal Cr(VI) ions in both times of contact, reaching almost 35 %. It is due to the reactions occurring at acidic pH, where the Cr(VI) forms the stable ions  $\text{HCrO}_4^-$  and  $\text{CrO}_4^{2-}$ .<sup>75</sup> Despite montmorillonite clay having a negatively charged surface due to the isomorphous substitutions occurring in the Si-O tetrahedrons or in the Al-O octahedrons<sup>75</sup>, different kind of oxides are present<sup>76</sup> and its point-zero charge (PZC) is between 4 and 6<sup>77</sup>.

Hence, at pH values lower than its PZC these oxides form aqua complexes (Figure 6.15) that turn the surface charge positive<sup>76</sup>, increasing the Cr(VI) anions adsorption on the surface.

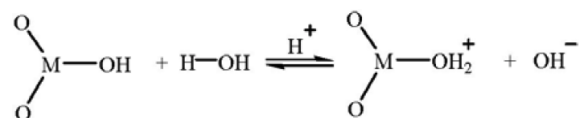


Figure 6.15 Oxides reaction at acidic pH. Extracted from Akar et. al<sup>74</sup>.

In the same way, in the case of the MOSP, it is rich in several functional groups from carbohydrates, proteins, cellulose, hemicellulose and lignin that conforms it; especially, the presence of carboxyl groups (-COOH)<sup>18</sup> and amine groups (-NH<sub>3</sub>)<sup>74</sup> which are very relevant for the adsorption of metal ions. Because both are protonated in an acidic pH, allowing their interaction with the anionic species of Cr(VI). MOSP has a PZC between 6 and 7, then, at lower pH values is favored the adsorption of anionic metals due to the positive charge on the surface of the MOSP<sup>18</sup>. For this reason, from Figure 6.16 is concluded that an acid pH has a better percentage of removal Cr(VI) ions, and also, the best composite is Composite 1.1 due to its higher composition of MOSP, increasing the number of functional groups that promote the adsorption of anions.

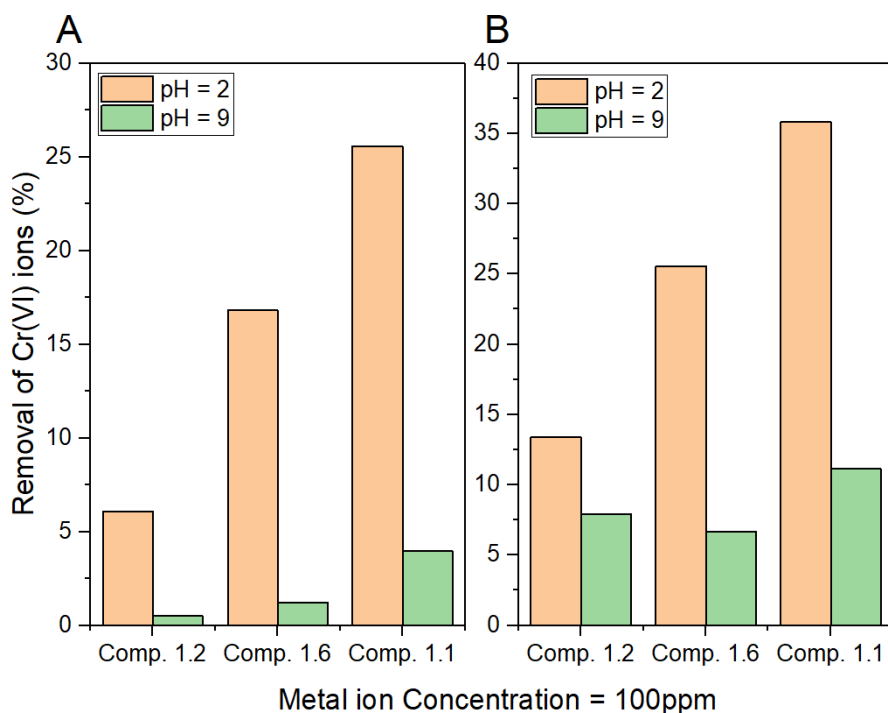


Figure 6.16 Effect of pH on the adsorption of Cr(VI) ions. Contact time: A. 1-hour B. 17 hours.

On the other hand, the removal ion percentage with pH = 9 showed very low results, not higher than 12 %. It is principally caused by the prevalence of OH<sup>-</sup> species at this pH, OH<sup>-</sup> competes with the Cr(VI) anions for the available adsorption sites<sup>75</sup> in the surface of the composites, decreasing the adsorption of the Cr(VI) anions. Also, at pH = 9 less functional groups will be protonated, reducing the electrostatic interactions with the Cr(VI) anions<sup>76</sup> and reducing the positively charged adsorption sites, hence, reducing the percentage of removal of Cr(VI) anions<sup>73</sup>. Besides, this basic pH is higher than the PZC value of montmorillonite clay and MOSP, increasing the negative charge of their surfaces, increasing the repulsion forces with the Cr(VI) anions<sup>18,76</sup>. Therefore, the suitable pH value selected for the next analysis is 2, that is an acidic medium.

### 6.6.2 Effect of contact time

To determine the most suitable contact time for the adsorption process, the percentage of removal Cr(VI) ions from the sample was considered. The test was performed at room temperature, with a constant adsorbent dose of 10 g/L, an initial Cr(VI) concentration of 100 ppm and a pH= 2. In this case, the three composites with diverse proportions of MOSP were tested at three different times of contact: 1 hour, 3 hours and 17 hours. Figure 6.17, shows that the adsorbed quantity of Cr(VI) ions increments with the increase of contact time. Between 1 hour and 3 hours adsorption is a remarkable difference, this fast adsorption results come from the numerous vacant adsorbent sites that are available at the start of the adsorption process<sup>78</sup>. As time passes, the adsorption gets slower, because the heat of adsorption starts to decrease as the work function gets higher (effort required to beat the repulsion interactions occurring in the surface); which is constantly increasing while the surface vacant sites are being filled<sup>73,79</sup>. Hence, the amount of Cr(VI) ions adsorbed start to reach an equilibrium state and that is why in Figure 6.17 it can be observed that there is not relevant difference in the percentage removal of Cr(VI) ions between 3 hours and 17 hours. For this reason, the most convenient contact time for the adsorption process in this work is 3 hours.

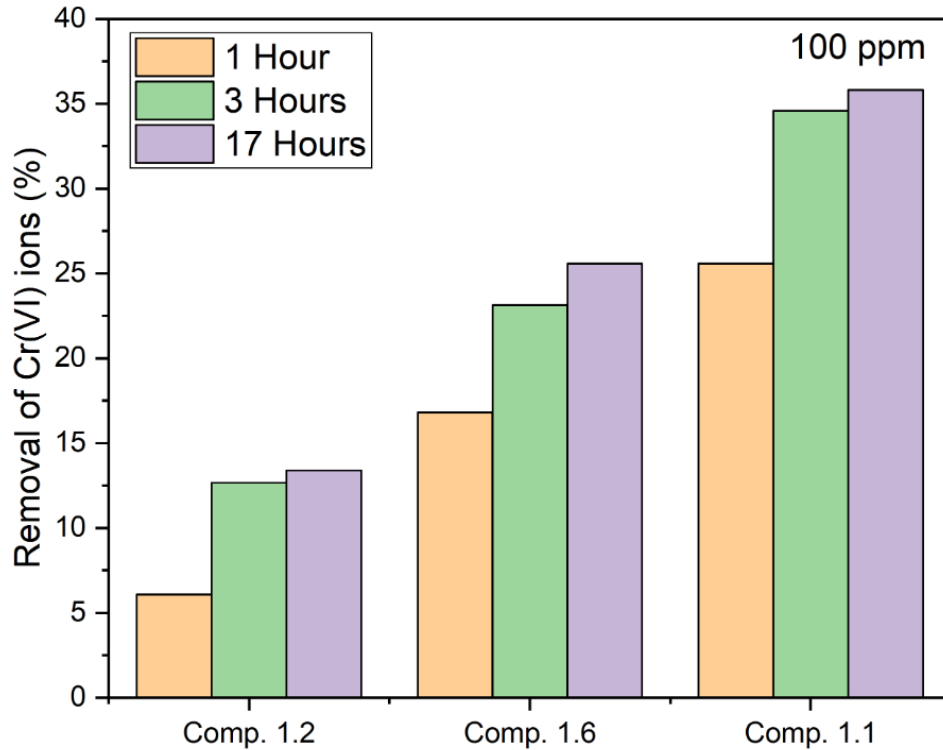


Figure 6.17 Effect of contact time in a 100ppm solution at 1h, 3h, and 17h.

### 6.6.3 Effect of initial metal ion concentration

This assessment was performed at room temperature, with a constant adsorbent dose of 10 g/L, an initial Cr(VI) concentration range from 100 ppm – 600 ppm, and a pH = 2. In Figure 6.18, a directly proportional relationship between the initial metal ion concentration ( $C_e$ ) and the adsorption capacity ( $q_e$ , in  $\text{mg}_{\text{chromium}}/\text{g}_{\text{adsorbent}}$ ) of the samples is observed. The case of the percentage of removal is a different situation, because there is an indirectly proportional relation between this percentage and the initial metal ion concentration. It happens because the higher the concentration, the more Cr(VI) ions are available to quickly adhere to the available adsorbent sites, hence, the adsorption capacity will increase<sup>78</sup>. While, for the inverse relation, it is caused by the higher concentration, the smaller is the ratio of the metal ions and available adsorbent sites, so it would be more ions competing for the few active sites that are available on the surface. In other words, if the concentration increase, the metal ions to be adsorbed increase too, but the amount of available adsorbent active sites remains the same reducing the percentage of removal ions from the solutions<sup>79</sup>. Besides, in Figure 6.18 is easy to observe the adsorption efficacy of each sample, being MOSP the most efficiency adsorbent for Cr(VI) ions. However, in

terms of composite, the best adsorbent is Composite 1.1 because it is the one with a higher composition of MOSP, turning Composite 1.1 in the best adsorbent synthesized in this work, even better than activated Na-montmorillonite.

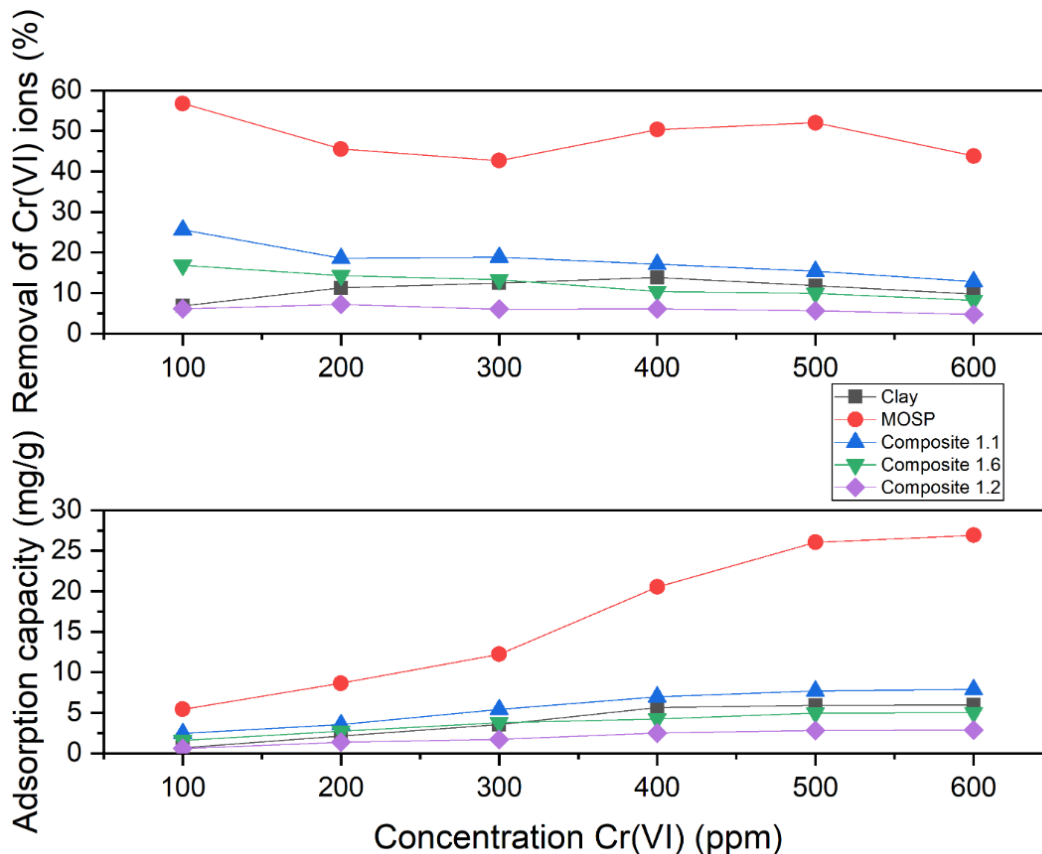


Figure 6.18 Effect of the initial Cr (VI) concentration in the adsorption capacity (mg/g) and removal efficiency (R %) of Cr (VI) ions (adsorbent dosage: 10 g/L, pH: 2 and reaction time: 3 h)

#### 6.6.4 Adsorption isotherms

The metal ions distribution between the liquid phase and the adsorbent surface during the adsorption process describes how equilibrium works, and can be explained through one or more adsorption isotherm models. Therefore, the adsorption data from different experiments carried out in this work were fitted according to isotherm of Langmuir and Freundlich, the more common models used to describe adsorption processes. Also, the data was tested using a previously reported modification of BET model to be extended for description of liquid<sup>53</sup>.

All prepared samples, such as activated Na-Montmorillonite (AMN), MOSP, and composite Comp-11, Comp-16 and Comp-12, were exposed to different Cr(VI) solutions, each

one with different initial concentrations, under the optimal conditions of pH and contact time determined in previous sections. Then, the capacity of the adsorption of each sample was evaluated. Table 6.3 shows a compilation of the obtained results, corresponding to the equilibrium concentration reached for the Cr(VI) species in solutions and their respective adsorbed amount of Cr(VI), which is denoted by  $q_e$  that express the adsorbed Cr(VI) milligrams per adsorbent grams.

Table 6.3 Adsorptive capacity obtained for each adsorbent evaluated for all of the chromium solutions.

Initial Concentration [ppm]	Adsorptive capacity ( $q_e$ ) [ $mg_{Cr(VI)}/g_{ads}$ ]				
	AMN	MOSP	Comp-11	Comp-16	Comp-12
100	0.651	5.419	2.442	1.605	0.581
200	2.140	8.651	3.535	2.721	1.372
300	3.558	12.209	5.395	3.791	1.721
400	5.651	20.512	6.977	4.233	2.488
500	5.907	26.023	7.698	4.953	2.814
600	5.977	26.907	7.884	5.000	2.884

From the values given in Table 6.3 the Langmuir, Freundlich, and BET-modified models were fitted according to equations 1 – 6. Langmuir and Freundlich adsorption isotherms fits for AMN and MOSP are shown in Figure 6.19 A and B, respectively. In these figures, poor fits for both models can be observed; this is possibly due to a heterogeneity surface, or a combination of occurring mechanisms simultaneously, that is, physisorption and chemisorption. Also, from these fits it is evident that solutions analyzed correspond to low chromium concentrations region, which does not allow establishing an unambiguous tendency of the behavior. In fact, Figure 6.20 shows an extrapolation for both models to higher concentration values, indicating that data obtained from this work is located at low concentration region of the plotted fits, in whose cases both models have similar behavior. From a concentration of 1000 ppm or higher it would be possible to notice a remarkable difference between both isotherms, but the values obtained in this work do not reach these chromium concentration values.

It is evident from the data showed in Table 6.3 that the highest adsorption capacity ( $q_e$ ) corresponds to the MOSP sample, which is corroborated by the  $N_T$  values, associated with the estimated amount of adsorbate to complete the monolayer on the surface, given in the Table 6.4.

It also shows that for MOSP around five times more adsorbate than for clay AMN is required to fill the complete surface ( $N_T$  in the Table 6.4).

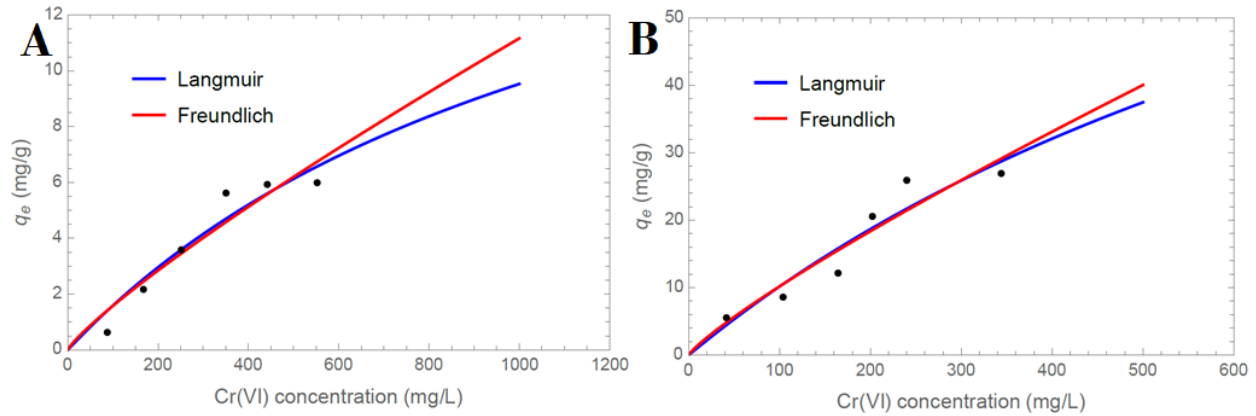


Figure 6.19 Isotherm data fit adjusted to isotherms Langmuir and Freundlich for (A) activated Na-montmorillonite clay (AMN) and (B) Moringa seeds powder (MOSP).

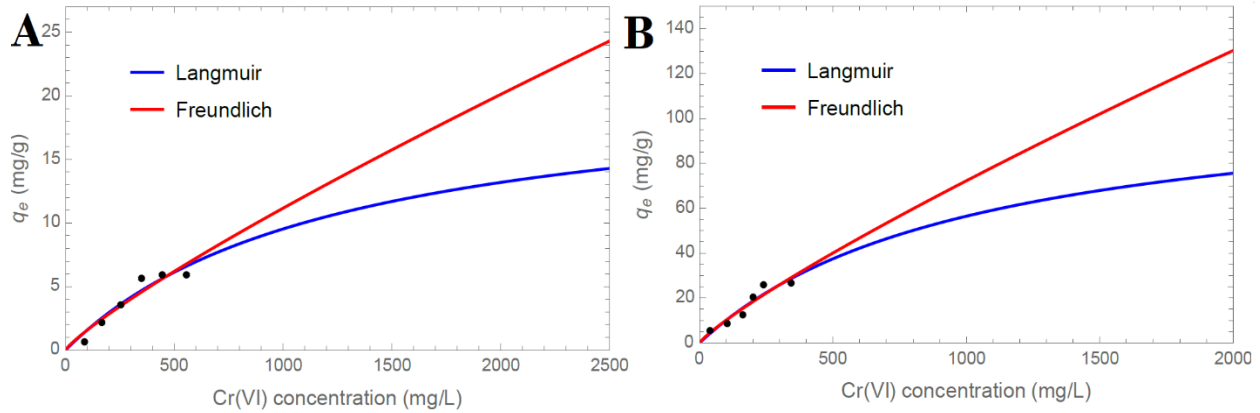


Figure 6.20 Isotherm data fit adjusted to isotherms Langmuir and Freundlich for (A) activated Na-montmorillonite clay (AMN) and (B) Moringa seeds powder (MOSP) at higher chromium concentrations.

As for the synthesized composites, the behavior changes slightly from the one described above. In Figure 6.21 the Langmuir and Freundlich fits for Comp-11 (A), Comp-16 (B) and Comp-12 (C) data are shown, this represents better fits for the Langmuir model, even for those estimated for higher chromium concentrations, as is plotted in Figure 6.22. This fact implies that the mechanism could be consistent with the formation of a monolayer on the composite surface, suggesting that some chemisorption processes is occurring, related to the presence of MOSP in the matrix clay, which has been previously suggested by XPS analysis. Also, the low capacity to form multilayers can be related to the pore volume decrease for the clay in the composites

indicated from the surface analysis results. This last consideration is associated with the composite's microporous material behavior.

In the case of the composite with the lowest proportion of MOSP (Comp-12) the adsorption capacity decreases due to the amount of the active sites on adsorbent for the Cr(VI) ions adsorption is reduced.

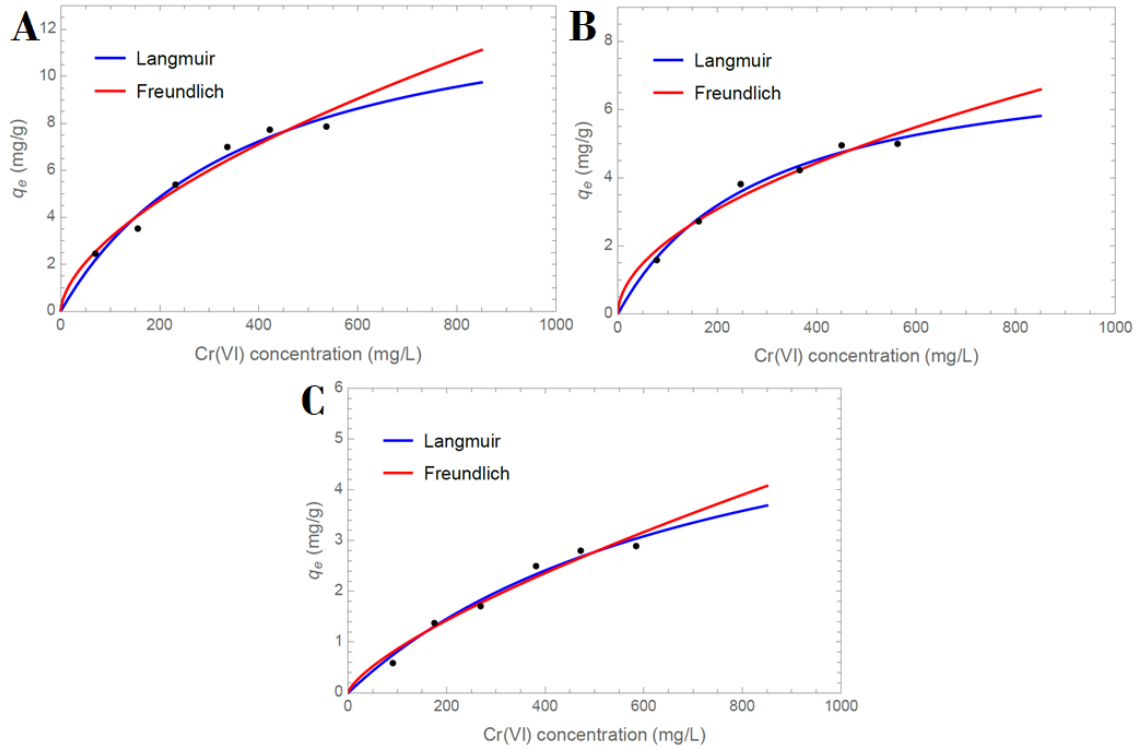


Figure 6.21 Isotherm data fit adjusted to isotherms Langmuir and Freundlich for A. Composite 1.1, B. Composite 1.6 and C. Composite 1.2

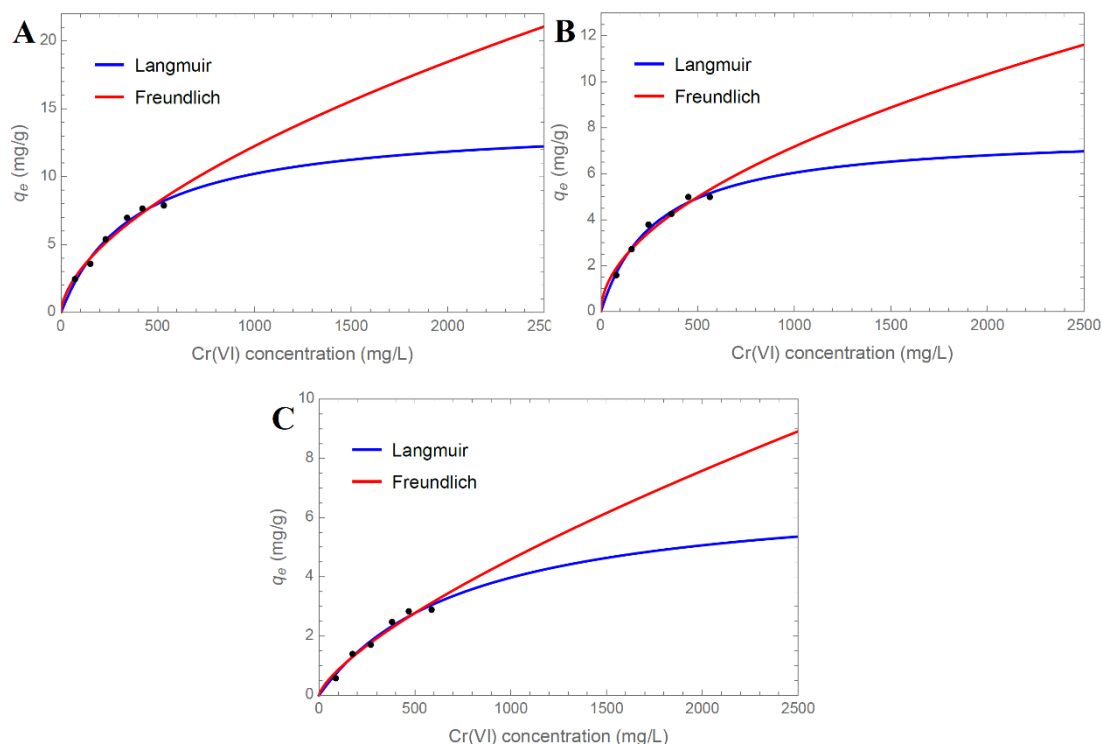


Figure 6.22 Isotherm data fitted to Langmuir and Freundlich model for (A) Comp-11, (B) Comp-16 and (C) Comp-12 at higher chromium concentrations.

In Table 6.4, the values obtained for fit parameters for Langmuir adsorption isotherm model for adsorbents evaluated are shown. These fit parameters correspond to  $K_L$  and  $N_T$ , according the equation 1, and related with the equilibrium constant of adsorption process and the required amount of adsorbate to fulfill the monolayer formation, respectively.

Table 6.4 Values for fit parameters associated with Langmuir Adsorption Isotherm for the different analyzed adsorbents.

Samples	Adsorption Isotherm Langmuir Parameters	
	$K_L$	$N_T$ [mgCr(VI)/g <sub>ads</sub> ]
AMN	0.80203	2.14
MOSP	0.97700	114.24
Comp-11	2.63133	14.09
Comp-16	3.47562	7.78
Comp-12	1.31799	6.98

The values from Table 6.4 expose the amount of Cr(VI) ions adsorbed in the solid, according Langmuir model. According these values, the adsorbent with highest capacity to remove chromium ions from aqueous solutions corresponds to MOSP, which can be deduced from the  $N_T$  value, that is, the total mg of Cr(VI) per gram of adsorbent required to fulfill the

surface of adsorbent. Moreover, by comparing the  $N_T$  values obtained for the AMN and for composites, the higher values for  $N_T$  obtained for composites confirm that the functionalization of AMN with the solution resulting from MOSP increases the adsorption capacity of the original clay. The adsorption capacity of the composite systematically increases with the content of MOSP material in the composite (Comp-11 has highest amount of MOSP, while the Comp-12 has the lowest one). On the other hand, the values for  $K_L$  parameters indicate a synergetic effect to improve the interaction between the chromium ions and composites surface.

When the modifications of BET model (equations 5 and 6) were tested, the experimental data presented even better fits. In the Figure 6.23 are shown both representations for Comp-11 adsorbent, that is, for the model using  $x = C_e/C_s$  (instead  $x = P/P^s$  as in the classical model) and for the equation 6, reported for the case of adsorbate liquid phase<sup>53</sup>.

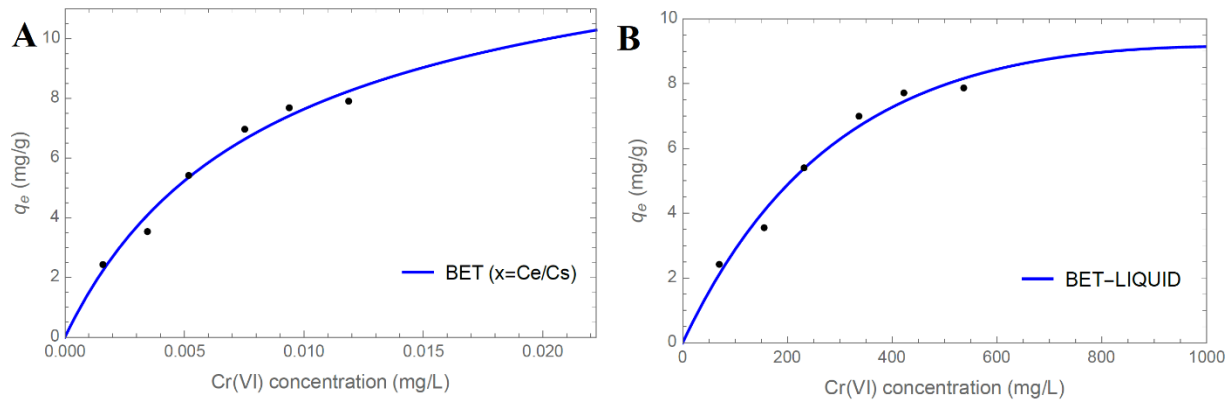


Figure 6.23 Adsorption isotherms Comp-11: (A) Classical BET model using  $x = C_e/C_s$  and (B) modified BET-model for liquids.

It is important to remember that BET model is usually applied to represent gaseous systems, as it was mentioned before, has been developed a modification of this model to extend its use to liquid model<sup>53</sup>, which is given in the equation 6. From the resulting fits were determined the parameters  $N_T$ , which has the same meaning as in the Langmuir model, and  $\kappa$  parameter associated with the adsorbate-adsorbent interaction strength (even for the classical BET model), and the parameters  $K_{ML}$ ,  $K_{UL}$ , associated with BET liquids model, representing the equilibrium constant of adsorption for the first layer and the upper layer, respectively.

Table 6.5 Values for fit parameters associated with both modified BET-models: Classical BET model using  $x = C_e/C_s$  and modified BET-model for liquids, for the different analyzed composites.

Samples	BET ( $x = C_e/C_s$ )		BET - LIQUIDS		
	$\kappa$	$N_T$ [ $mg_{Cr(VI)}/g_{ads}$ ]	$K_{ML}$	$K_{UL}$	$N_T$ [ $mg_{Cr(VI)}/g_{ads}$ ]
Composite 1.1	122.73	13.66	$1.90 \times 10^{-3}$	$7.4 \times 10^{-4}$	18.17
Composite 1.6	161.73	7.56	$2.28 \times 10^{-3}$	$9.19 \times 10^{-4}$	10.60
Composite 1.2	62.44	6.65	$1.10 \times 10^{-3}$	$4.17 \times 10^{-4}$	8.17

The values reported in Table 6.5 show fit parameters for both modified BET models for the adsorption of Cr(VI) ions on the prepared composites. According the values obtained, among the evaluated adsorbent, the one with highest adsorption capacity, and therefore with the capacity to remove the highest amount of Cr(VI) ions (per gram of adsorbent) from aqueous solution corresponds to Comp-11, which is consistent with the obtained results for Langmuir model. The values for  $N_T$  parameter for classical BET using  $x = C_e/C_s$  are closer to Langmuir model than those obtained for BET for liquids, although there are no significant differences. These results demonstrate that as the amount of MOSP in the composite increases, the adsorption capacity of the composite increases as well. Also, the good fit along the obtained curve shape, shown in the Figure 6.23, suggest that the presence of the MOSP in the surface of the composites contributes to the predominant adsorption mechanism being the chemisorption of the Cr(VI) ions on the composite surface, in agreement with the Langmuir model as it is observed and Figure 6.22. This affirmation is also confirmed by the lower value of the adsorption equilibrium constant for the upper layers ( $K_{UL}$ ) compare to that obtained for  $K_{ML}$ , which represents a higher difficult to form multilayers during the adsorption process. As for the interaction parameter ( $\kappa$ ) for the case of BET model with  $x = C_e/C_s$ , its increase may be associated with the presence of MOSP material on the adsorbent surface.

## Chapter 7

# Conclusions

Through this work, the functional groups of each evaluated adsorbent, that is, AMN, MOSP, and prepared composites were determined by the FT-IR Spectroscopy, confirming the preparation of composite from the combination of MOSP and the clay's matrix, due to the characteristic peak at  $1659.72\text{ cm}^{-1}$ , attributed to the carbonyl amides from protein content. In the same way, the EDX and XPS analysis confirmed the increase of carbon concentration in the composite compare to the clay's matrix, due to the MOSP presence in the composites. Besides, through the XRD diffractograms and the Surface Area analysis, it was confirmed that the preparation of composites was possible because of the adsorption of the MOSP in the clay's surface, but not for the absorption of the MOSP inside the clay's matrix. Hence, composites were successfully synthesized.

The adsorption results showed that all the samples: AMN, MOSP, and the three composites (Comp-11, Comp-16, and Comp-12) are capable of removal of Cr(VI) ions from aqueous solutions. The optimal conditions for that adsorption process were determined to be: 3 hours of contact time, an acid pH; which is required for the activation of the surface's functional groups and it works better at low concentrations of the metal ion.

According the results obtained from the adsorption analysis, MOSP is adsorbent with the highest removal of Cr(VI) ions with 56.75% at 100 ppm solution concentration, almost eight times more than AMN case (6.82%). While comparing the composites, Comp-11 shows the higher removal of Cr(VI) with 25.57%, almost four times more than AMN case. It affirms that the activation of AMN with MOSP increases the adsorption capacity of Cr(VI) ions in the natural clay.

The adsorption results suggest that the best composite for Cr(VI) ions adsorption is Comp-11, due to its high content of MOSP. It is inferred that the MOSP contributes to functional groups presence, such as carboxyl groups (-COOH) and amines groups (-NH<sub>3</sub>) on the composite

surface, increasing its interactions with the adsorbate. According to the data fits with the models of Adsorption Isotherms, a mechanism through the monolayer formation is suggested, with the subsequent physisorption process to the to the formation of multilayers, but in less proportion, reaching an equilibrium of sorption/desorption of the adsorbate. The monolayer formation may be attributed to chemisorption process due to MOSP – Cr(VI) interactions.

# References

1. Howard, G. & Bartram, J. *Domestic Water Quantity, Service, Level and Health*. World Health Organization (2003). doi:10.1016/S0009-9260(98)80189-X.
2. WHO (World Health Organization). *Guidelines for Drinking-water Quality*. vol. 91 (2017).
3. WHO (World Health Organization). & UNICEF. *Global Water Supply and Sanitation Assessment 2000 Report*. World Health Organization and United Nations Children's Fund Publications (2000). doi:10.1016/0273-1177(96)00073-7.
4. Gleick, P. H. World fresh water resources. in *Water in crisis: a guide to the World's Fresh Water Resources* 13–23 (Oxford University Press, 1993).
5. Mushtaq, N., Singh, D. V., Bhat, R. A., Dervash, M. A. & Hameed, O. Freshwater Contamination: Sources and Hazards to Aquatic Biota. *Fresh Water Pollut. Dyn. Remediat.* 27–50 (2020) doi:10.1007/978-981-13-8277-2.
6. Gleick, P. H. Global Freshwater Resources: Soft-Path Solutions for the 21st Century. *Science* (80-. ). **302**, 1524–1528 (2003).
7. WWAP (World Water Assessment Programme). *The United Nations World Water Development Report 3: Water in a Changing World*. (UNESCO, 2009). doi:10.1142/9781848160682\_0002.
8. Trösch, W. Water treatment. in *Technology Guide: Principles - Applications - Trends* 394–397 (2009). doi:10.1007/978-3-540-88546-7\_73.
9. Rozkosny, M., Kriska, M., Salek, J., Bodik, I. & Istenic, D. *Natural Technologies of Wastewater Treatment*. (2014).
10. Grim, R. E. & Kodame, H. Clay Mineral. *Encyclopedia Britannica* 2–4 (2014).

11. Faheem, U. Montmorillonite: An Introduction to Properties and Utilization. *Intech* 13 (2016) doi:<http://dx.doi.org/10.5772/57353>.
12. Shah, L. A. L. I. Industrial Application Suitability of Indigenous Bentonite Clay in Pharmaceutical Sector. (University of Peshawar, 2013).
13. Uddin, F. Clays, nanoclays, and montmorillonite minerals. *Metall. Mater. Trans. A Phys. Metall. Mater. Sci.* **39**, 2804–2814 (2008).
14. Adamis, Z. & Williams, R. B. Bentonite, kaolin, and selected clay minerals. *Environ. Heal. Criteria* (2005).
15. Sen Gupta, S. & Bhattacharyya, K. G. Adsorption of heavy metals on kaolinite and montmorillonite: A review. *Phys. Chem. Chem. Phys.* **14**, 6698–6723 (2012).
16. Shawky, H. A. Improvement of Water Quality Using Alginate/Montmorillonite Composite Beads. *J. Appl. Polym. Sci.* **116**, 2658–2667 (2010).
17. Olson, M. E. & Fahey, J. W. Moringa oleifera: Un árbol multiusos para las zonas tropicales secas. *Rev. Mex. Biodivers.* **82**, 1071–1082 (2011).
18. Araújo, C. S. T. *et al.* Bioremediation of Waters Contaminated with Heavy Metals Using Moringa oleifera Seeds as Biosorbent. *Intech* (2013).
19. TFL (Trees for Life). Moringa Book. in 1–52 (2010).
20. Bhatti, H. N., Mumtaz, B., Hanif, M. A. & Nadeem, R. Removal of Zn(II) ions from aqueous solution using Moringa oleifera Lam. (horseradish tree) biomass. *Process Biochem.* **42**, 547–553 (2006).
21. Oluwalana, S. A., Bankole, W., Bolaji, G. A. & Alegbeleye, O. Domestic water purification using Moringa oleifera Lam. *Niger. J. For.* **1**, 61–85 (1999).
22. Hernández, E. Uso de Moringa oleifera para el tratamiento de aguas. vol. 17 (Benemérita Universidad Autónoma de Puebla, 2017).

23. Alo, M. N., Anyim, C. & Elom, M. Coagulation and Antimicrobial Activities of Moringa oleifera Seed Storage at 3°C Temperature in Turbid Water. *Adv. Appl. Sci. Res.* **3**, 887–894 (2012).
24. Lédó, P. G. S., Lima, R. F. S., Paulo, J. B. A. & Duarte, M. A. C. Estudio comparativo de sulfato de aluminio y semillas de moringa oleifera para la depuración de aguas con baja turbiedad. *Inf. Tecnol.* **20**, 3–12 (2009).
25. Miller, R. G. *et al.* The Occurrence of Aluminum in Drinking Water. *Am. Water Work. Assoc.* **76**, 84–91 (1984).
26. Crapper, D. R., Krishnan, S. S. & Dalton, A. J. Brain Aluminum Distribution in Alzheimer ' s Disease and Experimental Neurofibrillary Degeneration. *Science (80-. )*. 511–513 (1973) doi:10.1126/science.180.4085.511.
27. Das, B. R., Kurup, P. A. & Narasimha Rao, P. L. Antibiotic Principle from Moringa Pterygosperma. *Naturwissenschaften* **9**, (1954).
28. Ross, I. A. Moringa pterygosperma. in *Medicinal Plants of the World* 367–381 doi:[https://doi.org/10.1007/978-1-59259-365-1\\_20](https://doi.org/10.1007/978-1-59259-365-1_20).
29. Arafat, M. G. & Mohamed, S. O. Preliminary study on efficacy of leaves, seeds and bark extracts of Moringa oleifera in reducing bacterial load in water. *Int. J. Adv. Res.* **1**, 124–130 (2013).
30. Abuye, C. *et al.* A compositional study of Moringa stenopetala leaves C. *East African Med. J.* **80**, (2003).
31. Burakov, A. E. *et al.* Adsorption of heavy metals on conventional and nanostructured materials for wastewater treatment purposes: A review. *Ecotoxicol. Environ. Saf.* **148**, 702–712 (2018).
32. Li, H., Liu, T., Li, Z. & Deng, L. Low-cost supports used to immobilize fungi and reliable technique for removal hexavalent chromium in wastewater. *Bioresour. Technol.* **99**, 2234–

- 2241 (2008).
33. FLACSO, MAE & PNUMA. GEO Ecuador 2008. Informe sobre el estado del medio ambiente. *Inf. sobre el estado del medio Ambient.* 192 (2008).
  34. Bhardwaj, V., Kumar, P. & Singhal, G. Toxicity of Heavy Metals Pollutants in Textile Mills Effluents. *Int. J. Sci. Eng. Res.* **5**, 664–666 (2014).
  35. Morais, S., Garcia e Costa, F. & Pereira, M. de L. Heavy Metals and Human Health. in *Environmental Health - Emerging Issues and Practice* vol. 22 227–246 (2012).
  36. ATSDR. Public Health Statement: Chromium. *Public Heal. Serv.* 1–9 (2012).
  37. Smith, A. H. & Steinmaus, C. M. Health Effects of Arsenic and Chromium in Drinking Water: Recent Human Findings. *Annu. Rev. Public Health* **30**, 107–122 (2009).
  38. Ministerio del Ambiente. REVISIÓN Y ACTUALIZACIÓN DE LA NORMA DE CALIDAD AMBIENTAL Y DE DESCARGA DE EFLUENTES : RECURSO AGUA. 1–40 (2015).
  39. Asamblea Nacional del Ecuador. Texto Unificado de Legislación Secundaria de Medio Ambiente, TULSMA. *Regist. Of. Edición Espec.* 2 31-mar.-2003 1–578 (2003).
  40. The Editors of Encyclopaedia Britannica. Adsorption. *Encyclopedia Britannica* (2013).
  41. Artioli, Y. Adsorption. *Encyclopedia of Ecology* 60–65 (2008) doi:10.1016/B978-008045405-4.00252-4.
  42. Vieira, A. M. S. *et al.* Use of Moringa oleifera seed as a natural adsorbent for wastewater treatment. *Water. Air. Soil Pollut.* **206**, 273–281 (2010).
  43. Shen, D. *et al.* Adsorption kinetics and isotherm of anionic dyes onto organo-bentonite from single and multisolute systems. *J. Hazard. Mater.* **172**, 99–107 (2009).
  44. Ayawei, N., Ebelegi, A. N. & Wankasi, D. Modelling and Interpretation of Adsorption

- Isotherms. *J. Chem.* **2017**, (2017).
45. Unuabonah, E. I., Omorogie, M. O. & Oladoja, N. A. *Modeling in Adsorption: Fundamentals and Applications. Composite Nanoadsorbents* (Elsevier Inc., 2019). doi:10.1016/b978-0-12-814132-8.00005-8.
  46. Ma, X. *et al.* Adsorption of heavy metal ions using hierarchical CaCO<sub>3</sub>-maltose meso/macroporous hybrid materials: Adsorption isotherms and kinetic studies. *J. Hazard. Mater.* **209–210**, 467–477 (2012).
  47. Matshitse, R. Brunauer-Emmett-Teller (BET) surface area analysis. *Rhodes Univ. Natl. Res. Found.* (2010).
  48. Brame, J. A. & Griggs, C. Surface Area Analysis Using the Brunauer-Emmett-Teller (BET) Method. *Eng. Res. Dev. Cent.* 1–23 (2016) doi:39180-6199.
  49. Condon, J. *Surface Area and Porosity Determinations by Physisorption. Measurements and Theory.* (2006).
  50. Aligizaki, K. *Pore Structure of Cemen-Based Materials: testing, interpretation and requirements.* (2005).
  51. De Smedt, C., Ferrer, F., Leus, K. & Spanoghe, P. Removal of pesticides from aqueous solutions by adsorption on zeolites as solid adsorbents. *Adsorpt. Sci. Technol.* **33**, 457–485 (2015).
  52. Rangabhashiyam, S., Anu, N., Giri Nangagopal, M. S. & Selvaraju, N. A Novel approach of the modified BET isotherm towards continuous column study. *J. Sci. Ind. Res. (India)*. **73**, 489–494 (2014).
  53. Ebadi, A., Soltan Mohammadzadeh, J. S. & Khudiev, A. What is the correct form of BET isotherm for modeling liquid phase adsorption? *Adsorption* **15**, 65–73 (2009).
  54. Pagnanelli, F., Mainelli, S., Vegliò, F. & Toro, L. Heavy metal removal by olive pomace:

- Biosorbent characterisation and equilibrium modelling. *Chem. Eng. Sci.* **58**, 4709–4717 (2003).
55. Nand, V., Maata, M., Koshy, K. & Sotheeswaran, S. Water Purification using *Moringa oleifera* and Other Locally Available Seeds in Fiji for Heavy Metal Removal. *Int. J. Appl. Sci. Technol.* Vol. **2**, 125–129 (2012).
  56. Obuseng, V., Nareetsile, F. & Kwaambwa, H. M. A study of the removal of heavy metals from aqueous solutions by *Moringa oleifera* seeds and amine-based ligand 1,4-bis[N,N-bis(2-picoyl)amino]butane. *Anal. Chim. Acta* **730**, 87–92 (2012).
  57. Sharma, P., Kumari, P., Srivastava, M. M. & Srivastava, S. Removal of cadmium from aqueous system by shelled *Moringa oleifera* Lam. seed powder. *Bioresour. Technol.* **97**, 299–305 (2006).
  58. Alves, V. N. *et al.* Determination of cadmium in alcohol fuel using *Moringa oleifera* seeds as a biosorbent in an on-line system coupled to FAAS. *Talanta* **80**, 1133–1138 (2010).
  59. Bergaya, F., Theng, B. K. & Lagaly, G. *Handbook of Clay Science. Elsevier Science* vol. 1 (2006).
  60. Flores, L. & Alcalá, R. *Manual de Procedimientos Analíticos: Física de Suelos. Instituto de Geología* (2010). doi:10.1007/s00431-003-1251-6.
  61. Bastardo-González, E., Deyán, C. C. & Brito, J. L. Acid activated pillared clays with aluminum as CoMo catalysts support for the hydrodesulphurization of thiophene. *Rev. Tec. la Fac. Ing. Univ. del Zulia* **41**, 95–103 (2018).
  62. Taffarel, S. R. & Rubio, J. On the removal of Mn<sup>2+</sup> ions by adsorption onto natural and activated Chilean zeolites. *Miner. Eng.* **22**, 336–343 (2009).
  63. Bhutada, P. R., Jadhav, A. J., Pinjari, D. V., Nemade, P. R. & Jain, R. D. Solvent assisted extraction of oil from *Moringa oleifera* Lam. seeds. *Ind. Crops Prod.* **82**, 74–80 (2016).

64. Tukki, O. H., Barminas, J. T., Osemeahon, S. A., Onwuka, J. C. & Donatus, R. A. Adsorption of colloidal particles of Moringa oleifera seeds on clay for water treatment applications. *J. Water Supply Res. Technol. - AQUA* **65**, 75–86 (2016).
65. Akpomie, K. G. & Dawodu, F. A. *Efficient abstraction of nickel(II) and manganese(II) ions from solution onto an alkaline-modified montmorillonite. Journal of Taibah University for Science* vol. 8 (Taibah University, 2014).
66. Cottet, L. *et al.* Adsorption characteristics of montmorillonite clay modified with iron oxide with respect to methylene blue in aqueous media. *Appl. Clay Sci.* **95**, 25–31 (2014).
67. Mindat.org. Montmorillonite. <https://www.mindat.org/min-2821.html>.
68. Yang, S. *et al.* Competitive sorption and selective sequence of Cu(II) and Ni(II) on montmorillonite: Batch, modeling, EPR and XAS studies. *Geochim. Cosmochim. Acta* **166**, 129–145 (2015).
69. RRUFF.info. Montmorillonite X-ray Data.
70. Moulder, J., Stickle, W., Sobol, P. & Bomben, K. *Handbook of X-ray Photoelectron Spectroscopy*. (1992).
71. Xiao, S. *et al.* Layer-by-layer assembly of polyelectrolyte multilayer onto PET fabric for highly tunable dyeing with water soluble dyestuffs. *Polymers (Basel)*. **9**, (2017).
72. Mäntele, W. & Deniz, E. UV–VIS absorption spectroscopy: Lambert-Beer reloaded. *Spectrochim. Acta - Part A Mol. Biomol. Spectrosc.* **173**, 965–968 (2017).
73. Timbo, C. C., Kandawa-Schulz, M., Amuanyena, M. & Kwaambwa, H. M. Adsorptive Removal from Aqueous Solution of Cr(VI) by Green Moringa Tea Leaves Biomass. *J. Encapsulation Adsorpt. Sci.* **07**, 108–119 (2017).
74. Fan, D., Zhu, X., Xu, M. & Yan, J. Adsorption properties of chromium (VI) by Chitosan Coated Montmorillonite. *J. Biol. Sci.* **6**, 941–945 (2006).

75. Yuan, P. *et al.* Montmorillonite-supported magnetite nanoparticles for the removal of hexavalent chromium [Cr(VI)] from aqueous solutions. *J. Hazard. Mater.* **166**, 821–829 (2009).
76. Akar, S. T., Yetimoglu, Y. & Gedikbey, T. Removal of chromium (VI) ions from aqueous solutions by using Turkish montmorillonite clay: effect of activation and modification. *Desalination* **244**, 97–108 (2009).
77. Helmy, A. K., Ferreiro, E. A. & De Bussetti, S. G. Cation exchange capacity and condition of zero charge of hydroxy-Al montmorillonite. *Clays Clay Miner.* **42**, 444–450 (1994).
78. Wang, G. *et al.* Cr(VI) adsorption by montmorillonite nanocomposites. *Appl. Clay Sci.* **124–125**, 111–118 (2016).
79. Sasikala, S. & Muthuraman, G. Chromium(VI) Removal Using Biosorbents Derived from *Moringa Oleifera*. *Ind. Chem.* **01**, (2015).

# Annex 1

## FT-IR Analysis for Composites

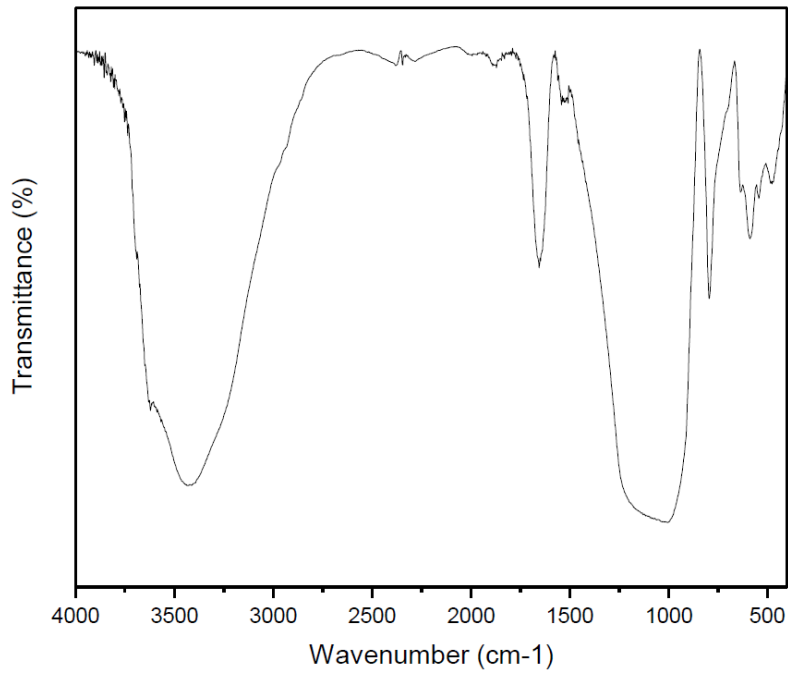


Figure 7.1 FT-IR spectra of Composite 1.6

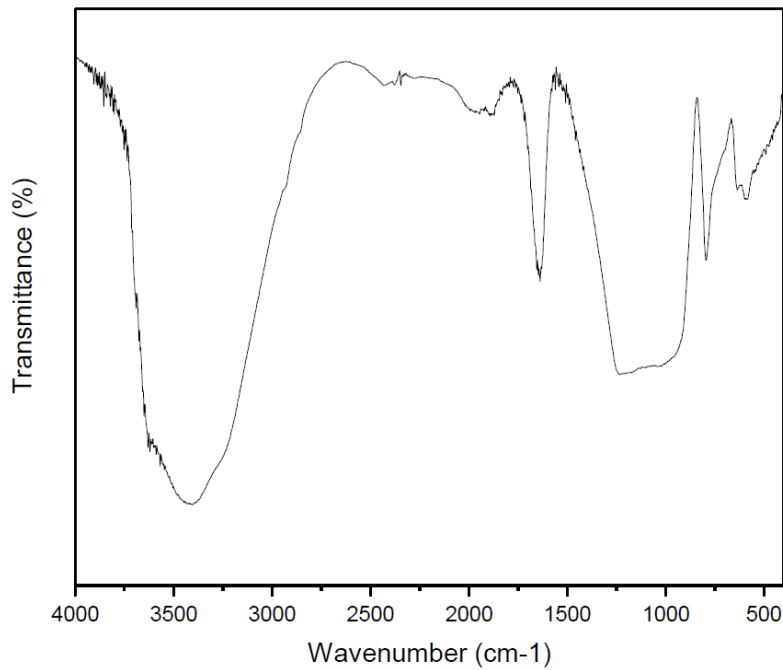


Figure 7.2 FT-IR spectra of Composite 1.2

# Annex 2

## Adsorption Isotherms by Modified BET model for composites Comp-16 and Comp-12.

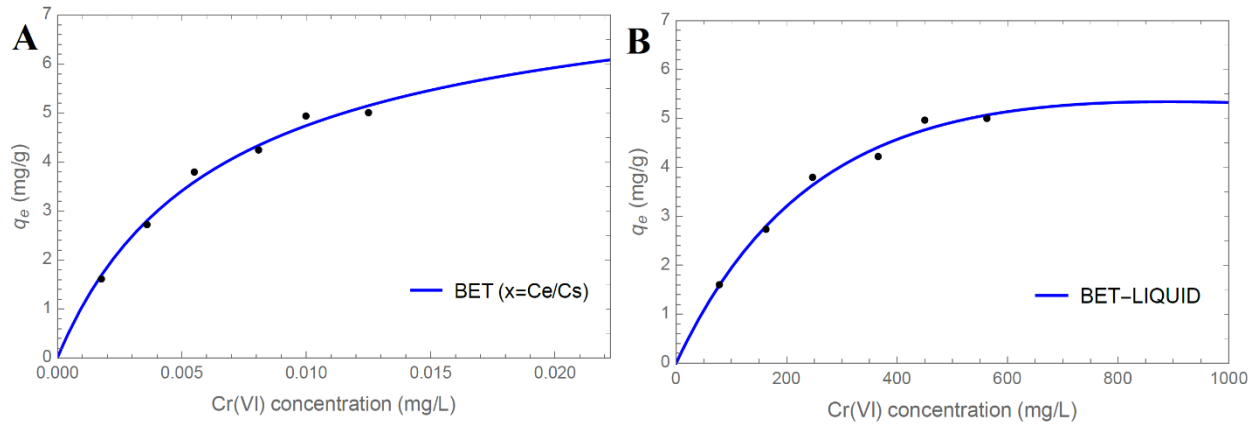


Figure 7.1 BET Adsorption isotherms Comp-16: (A) Classical BET model using  $x = C_e/C_s$  and (B) modified BET-model for liquids.

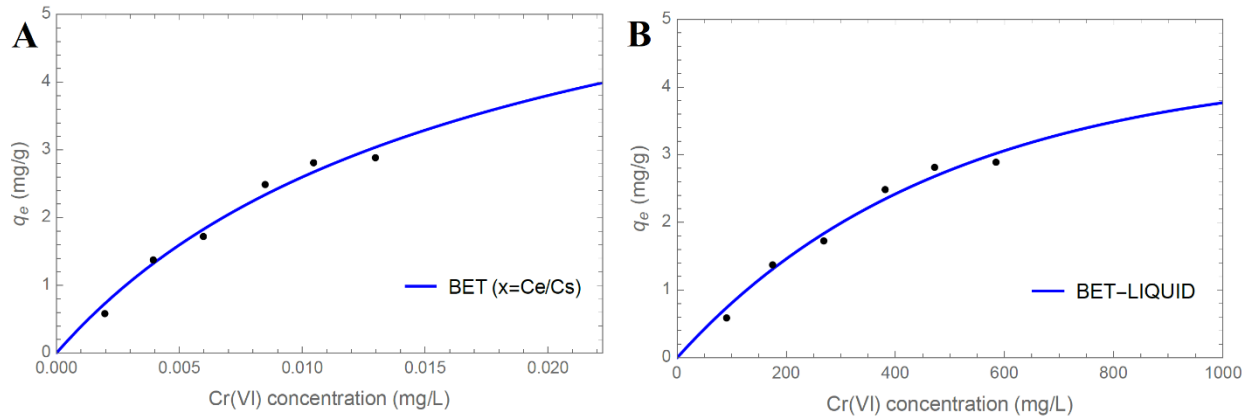


Figure 7.2 BET Adsorption isotherms for Comp-12: (A) Classical BET model using  $x = C_e/C_s$  and (B) modified BET-model for liquids.

# Annex 3

Removal of Cr(VI) ions (%) of all the materials analyzed.

*Table 7.1 Removal of Cr(VI) ions of all materials used (%)*

Initial Concentration (ppm)	% Removal of Cr(VI) ions				
	Clay	MOSP	Composite 1.1	Composite 1.6	Composite 1.2
100	6.82	56.75	25.57	16.80	6.09
200	11.27	45.55	18.61	14.33	7.23
300	12.43	42.66	18.85	13.25	6.01
400	13.87	50.35	17.13	10.39	6.11
500	11.81	52.03	15.39	9.90	5.63
600	9.74	43.83	12.84	8.15	4.70